FIELD MONITORING AND NUMERICAL ANALYSIS OF TWO ILLINOIS INTEGRAL ABUTMENT BRIDGES

BY

GABRIELA BRAMBILA

THESIS

Submitted in partial fulfillment of the requirements
for the degree of Master of Science in Civil Engineering
in the Graduate College of the
University of Illinois at Urbana-Champaign, 2017

Urbana, Illinois

Advisers:

Associate Professor Larry A. Fahnestock
Professor James M. LaFave

ABSTRACT

As compared to conventional jointed bridges, integral abutment bridges (IABs) require lower construction and maintenance costs and have a longer service life, leading to their increased use by Departments of Transportation in the U.S. However, due to their unique design, their structural behavior is not as fully understood as that of typical jointed bridges. Previous research on IABs has been heavily focused on substructure performance, leaving a need for better understanding of IAB superstructure behavior and interdependent effects. The aims of this project were to further investigate IAB structural behavior, particularly of the superstructure, under thermal loading and validate employed modeling assumptions through implementation of a field monitoring program. Two Illinois IABs were instrumented to monitor: i) global bridge movements, ii) pile, deck, girder, and approach slab strains, and iii) rotations at different abutment interfaces. Field monitoring results corroborate that IAB longitudinal expansion and contraction is somewhat less than theoretical free expansion and contraction, and is influenced by bridge skew. Pile strain values were below the yield limit and indicate there is likely some reserve pile deformation capacity typically available. Significant girder stresses due to thermal loading were observed, particularly at the girder bottom flange, which can be considered in design. Results indicate the abutment cold joint behaves as a rigid connection, while the girder-abutment connection displays a slight amount of differential rotation. Overall field results and corresponding bridge numerical models provide valuable insight into different aspects of IAB behavior and validate key modeling assumptions, indicating the potential for further application of the field monitoring and prior parametric study results in future IAB designs.

ACKNOWLEDGMENTS

This thesis is based in part on the project ICT R27-115, Analysis of Superstructures of Integral Abutment Bridges. ICT R27-115 is being conducted in cooperation with the Illinois Center for Transportation (ICT); IDOT, Division of Highways; the Illinois State Tollway Authority (ISTA); and the U.S. Department of Transportation, Federal Highway Administration (FHWA). The contents of this thesis reflect the view of the author, who is responsible for the facts and the accuracy of the data presented herein. The contents do not necessarily reflect the official views or policies of the ICT, IDOT, ISTA or FHWA. I would like to thank the members of the project Technical Review Panel, chaired by Mark D. Shaffer of the Illinois Department of Transportation, for their valuable assistance.

Additionally, I would like to acknowledge all past researchers who have contributed to this project: Beth A. Wright, Matthew W. Jarrett, Jeffrey S. Svatora, Joseph K. Riddle, and Huayu An. I would especially like to thank my advisers Associate Professor Fahnestock and Professor LaFave. They were always very encouraging and supportive of my work and have helped me become a better student, researcher, and professional.

Finally, I must express my profound gratitude to my parents, my brother, and to my friends for their unconditional support and encouragement throughout my years of study. This accomplishment would not have been possible without them. Thank you.

TABLE OF CONTENTS

CHAPTER 1: INTRODUCTION

Many Departments of Transportation (DOT's) throughout the country are increasing their use of integral abutment bridges (IABs) due to their extended service life and lower maintenance and construction costs (Arsoy et al. 1999; Hassiotis et al. 2006). An IAB differs from a conventional jointed bridge since in an IAB the abutment and deck are cast monolithically, and the girders and piles are embedded into the abutment, as shown in Figure 1. Therefore, IAB structural behavior is different than that of conventional bridges, as the superstructure and substructure of an IAB behave as one continuous unit under thermal loads.

IAB design practice varies widely throughout the country, largely due to the fact that IAB behavior is more difficult to analyze because of its continuous structural form. As the behavior of these bridges is still not completely understood, several states (including Illinois) have pursued research projects regarding IABs. At the University of Illinois two previous projects were conducted on IABs, however focusing on investigating substructure behavior. Similarly, much of the previous research conducted on IABs has focused on substructure behavior, and thus most design guidelines are based on substructure demands. Many uncertainties still remain regarding IAB superstructure behavior and design, which provided the motivation for this research project regarding overall IAB behavior, with an emphasis on thermal loads and superstructures.

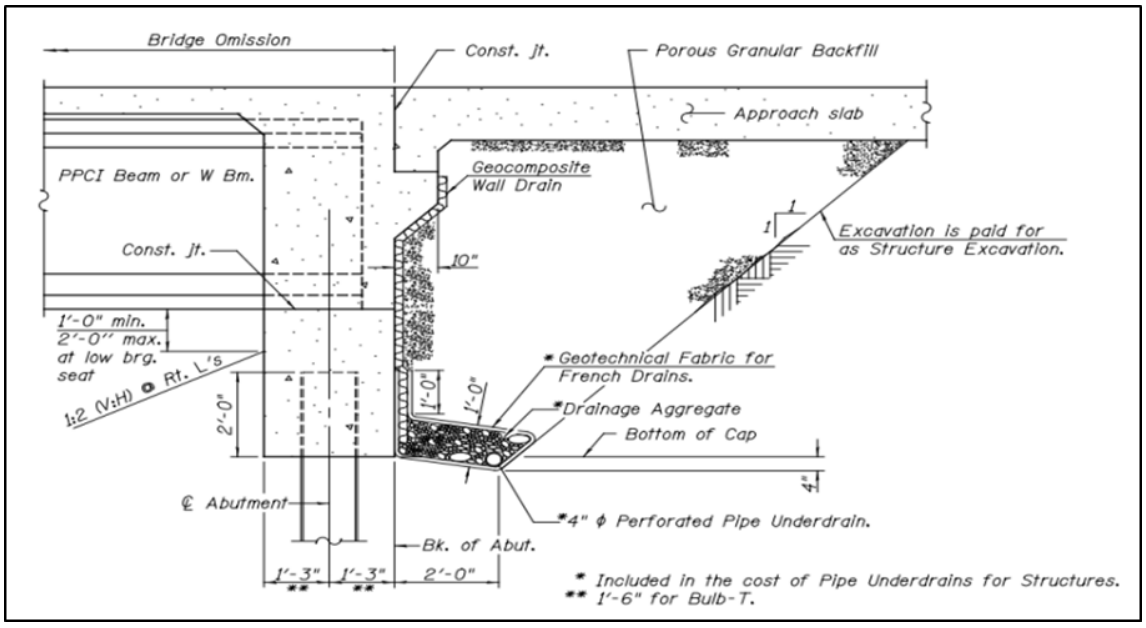

Figure 1. Typical Illinois Department of Transportation IAB Detail.

The objective of the overall project has been to further investigate IAB thermal behavior, particularly on superstructures, with the goal of providing improved design and construction provisions for IABs. To do so, the overall research project was comprised of a comprehensive parametric study utilizing finite element (FE) bridge models and field monitoring of two (2) IABs in Illinois. The parametric study was previously completed and its findings are summarized in LaFave et al. (2016). This thesis focuses on the field instrumentation and monitoring of two Illinois I-90 mainline (Illinois Tollway) IABs, the Union Pacific Railroad (UPRR) Bridge and the Kishwaukee River Bridge, shown in Figure 2. The superstructure and substructure of both bridges were instrumented as part of the field monitoring program. The main goals of the field monitoring program were to validate key modeling assumptions, corroborate findings from the parametric study, and more accurately capture different aspects of IAB behavior that are exhibited in the field.

Figure 2: Kishwaukee River Bridge (left) and Union Pacific Rail Road Bridge (right).

To supplement the field monitoring effort, finite element (FE) models were created for each of the instrumented bridges. These models were created utilizing the same assumptions and design procedure as the models from the parametric study, as will be further discussed in Chapter 5. Comparison of the field and model results of the instrumented bridges allowed for evaluation of modeling assumptions implemented for the instrumented bridge models and previous parametric study models. FE model results also provided a point of comparison for the field results allowing for further analysis of the field data. Field results were also compared to previous findings from the related parametric study. (A brief summary of the parametric study findings is included in Chapter 3). This thesis details the implementation of the field monitoring program and summarizes results from both the field data and instrumented bridge FE models.

CHAPTER 2: LITERATURE REVIEW

Only a limited amount of research has been conducted on IAB superstructures. Most of the research effort, including previous research conducted at the University of Illinois, has been focused on substructure behavior and design. This chapter briefly summarizes previous IAB research conducted at Illinois, previous field monitoring research regarding IABs, and work specific to site conditions relevant to the current project.

2.1 PREVIOUS ILLINOIS IAB RESEARCH

Previously at Illinois, a two-phase project was conducted focusing on IAB substructure behavior and design. The first phase consisted of a 2-dimensional (2-D) and 3-dimensional (3-D) parametric study which was completed in August 2009 (Olson et al. 2009). It was concluded that the type of girders, pile soil, and the development of abutment backfill passive pressure cause secondary effects on the pile foundation performance. The use of compacted granular backfill was recommended, along with several possible options to reduce pile moments in order to reduce length and skew limitations. In addition, the substructure of two bridges were instrumented and monitored to validate modeling assumptions.

The second phase of the project included a more extensive 3-D parametric study (Olson et al. 2012). The study recommended that IDOT should consider combined length and skew effects. It was concluded that thermal loading, combined with live loading, would create the maximum demands on piles. Time-dependent effects were investigated on a limited basis, however, the importance of shrinkage and creep were emphasized. This could significantly alter bridge long-term behavior from considering only thermal and live loadings. One thing to note is that the study did not take into account pile plasticity, now commonly assumed in IAB design in many other states. Additionally, the study limited pile head stress to the "first yield" limit state, which has since been updated by IDOT. The study did not consider superstructure behavior and thus the recommendations were based only on substructure behavior and demands. Therefore, this gap in understanding of IAB superstructure behavior led to this current project focused on IAB superstructure behavior under thermal loading.

2.2 IAB FIELD MONITORING RESEARCH

The integral construction inherent in IABs significantly increases substructure demands, which has caused much of the primary focus of IAB research to be on substructure behavior and demands. Dicleli (2004), Ingram et al. (2004) and Paul et al. (2005) all found that IAB effective expansion length (EEL) has significant influence on IAB behavior since both global bridge superstructure movement and pile displacement demand are directly related to EEL. Other primary factors identified to have an effect on IAB pile behavior and overall bridge response to thermal loading include backfill soil stiffness, pile soil stiffness, and the superstructure itself (Dicleli 2005). IAB superstructure and substructure behavior are further interrelated as mentioned by Burdette et al. (2004), Kim and Laman (2010), and Olson et al. (2012). Many previous studies regarding IABs are heavily comprised of analytical results, however other research efforts employing field monitoring of IABs have provided some further insight to complement previous analytical findings regarding IABs, as briefly outlined below.

In a study conducted in New Jersey a two-span high-performance steel girder IAB was monitored with the purpose of investigating abutment displacements and the effect of relevant design parameters on pile forces and pile-soil interaction (Khodair and Hassiotis 2013). The bridge was instrumented with strain gages to measure strains at different depths of the piles, tiltmeters to measure rotations at the abutment – girder connections, thermocouples to measure temperature variations throughout the deck, displacement transducers to measure displacement of the relief slab, and soil pressure cells to measure pressure on the pile sleeves behind the abutment. Field results showed that increases in abutment rotation due to temperature change resulted in an increase in pile axial forces. Due to larger transverse movement of the bridge's obtuse side, an increase in soil pressure at this location was also observed, resulting in higher axial stresses in the piles near the obtuse side.

Pennsylvania State University (Paul et al. 2005) explored IAB superstructure behavior due to thermal loading through field monitoring and parametric analysis. The top and bottom of a prestressed concrete slab-on-beam bridge was instrumented and monitored. Additionally, a 2-D parametric analysis was conducted, which confirmed that substantial superstructure forces can be induced by thermal loading. Significant girder forces were observed in the field data, however there are several different possible factors affecting these girder forces in the field, which are

difficult to isolate. Additionally, results from both the numerical analysis and the field data indicated that creep and shrinkage may have had a substantial effect on girder forces, and that thermally induced stresses may lead to cracking in concrete IABs. Results also showed that thermally induced girder forces increase with an increasing EEL a show in Figure 3.

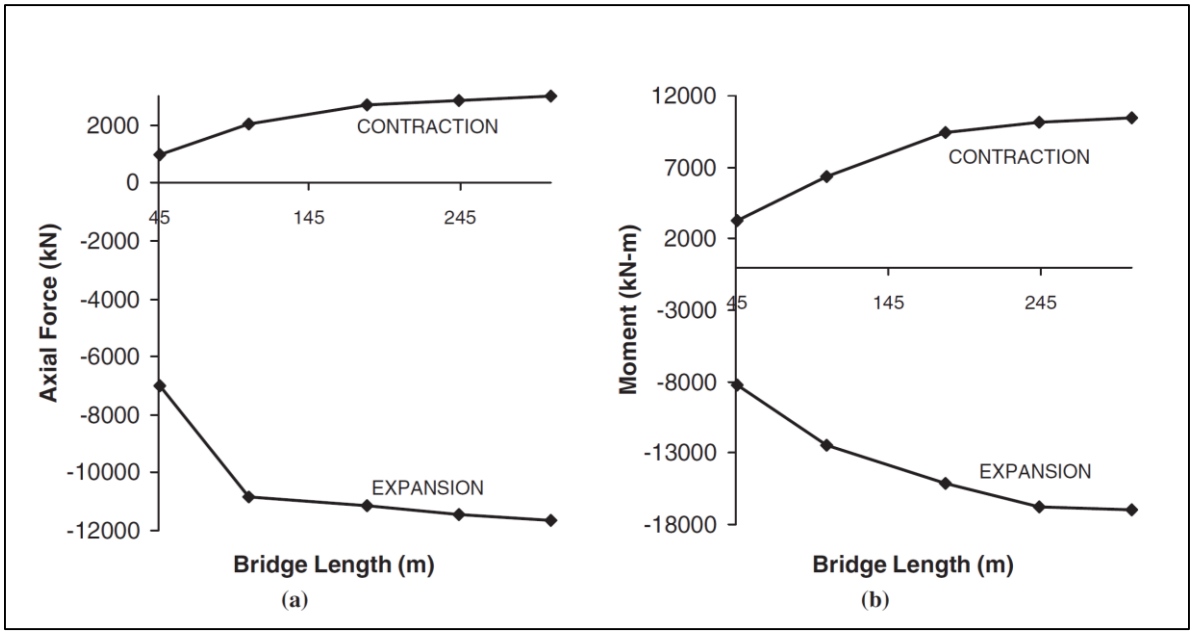

Figure 3. Thermally-induced girder axial force and moment as a function of concrete IAB length (Paul et al. 2005, Figure 8).

Further longer-term monitoring was conducted in Pennsylvania in a study that included the monitoring of four (4) short to medium-long concrete girder IABs for seven (7) years (Kim and Laman 2012). The goal of the field monitoring was to track long-term trends of abutment displacement, backfill pressure, abutment rotation, girder rotation, girder forces, pile forces, and approach slab strains. Analysis of abutment displacement results from all four bridges exhibited an increase in unrecoverable total abutment movement. Analysis of the rotation results indicated some differential rotation between the girders and abutment, indicating that the girder – abutment connection is not entirely rigid. Significant girder moments and axial forced induced by thermal loading were observed, and thus it was recommended they be considered in design. Further comparison to FE models of the four (4) IABs revealed that girder axial forces are largely influenced by end-span length, as opposed to solely by overall bridge length (Kim and Laman 2010).

In West Virginia, a three-span steel girder IAB was instrumented and monitored with the goal of observing abutment movement and its corresponding effect on superstructure stresses due to thermal loading (Shoukry et al. 2008). Strain gages were placed at different locations throughout the bridge deck and along three girders, along with crackmeters to measure relative movement of the supports and bridge joints. Strain results from the girder top and bottom flanges demonstrated clear seasonal trends over time and the strain readings indicated these trends are caused primarily by temperature changes and the weight of the bridge deck. Analysis of field data allowed for calculation of girder bending moments, which showed close agreement with theoretical bending moment values. The calculated axial forces in the girders due to passive backfill pressure were significant, and thus it was recommended to account for this in the design of bridge superstructures. These findings are supported by those from William et al. (2012), which found that significant girder forces are induced due to restraint of the abutment by the backfill and supporting piles. In most typical IAB bridge design procedures these forces are not explicitly considered.

Additional long-term effects were observed by Huang et al. (2004) in Minnesota in a study consisting of field monitoring of a concrete prestressed girder IAB, through instrumentation of various cross-sections of the superstructure. Field results demonstrated a decrease in girder strains over the years, which was attributed to creep and shrinkage effects. Variations in girder strain across cross sections at difference bridge locations were observed and explained, however no recommendation was provided regarding modifications of IAB superstructure design. In Indiana, another long-term field monitoring program implemented on three (3) different IABs also demonstrated "ratcheting" of contraction displacements due to deck shrinkage. The amount of shrinkage observed due to ratcheting was greater than that due to thermal contraction (Frosch and Lovell 2011). Although important, due to uncertainty regarding modeling of these time-dependent demands, such effects have not been incorporated into the numerical models of the project this thesis reports on.

2.3 SPECIFIC SITE CONDITIONS

There are other more specific topics regarding bridge and site conditions in relation to IABs which have only been investigated on a more limited basis, including some debated topics such as pile orientation, pile head fixity, and pile relief. These three conditions are relevant to one or both of

the instrumented bridges in this project. These specific conditions were only partially assessed (if implemented at all) in the project's prior parametric study. As part of the secondary parameter analysis of the parametric study, pile orientation was explored on a limited basis (LaFave et al. 2016). It was concluded that orienting the piles in so-called weak-axis orientation imposed smaller magnitude built-up superstructure forces as compared to strong-axis oriented piles. This is due to the fact that weak-axis oriented piles maximize the bridge expansion and contraction; however, this does allow for more plastification at the pile head to occur due to larger pile deformations. On the other hand, utilizing strong-axis oriented piles resulted in increased foundation stiffness, thus reducing peak pile strains but increasing girder internal forces. It was thus concluded that it is important to consider effects on both the substructure and superstructure when determining an appropriate pile orientation.

A parametric study conducted by Quinn and Civjan (2017) investigating pile orientation also concluded that there is no single optimal pile orientation, but rather, that the optimal orientation for any particular IAB is dependent on several factors. The parametric study investigated different combinations of degrees of skew with both strong-axis and weak-axis pile orientation for single-span bridges subjected to thermal loading. Parametric study results indicated that construction temperature, and minimum and maximum design temperatures are important factors to consider in determining the appropriate pile orientation, as they play a role in determining if transverse movement is greater in contraction or expansion. The study recommended that construction and minimum and maximum design temperatures, along with backfill conditions, bridge length, and skew, be considered in the selection of pile orientation.

Another aspect important in IAB behavior is direct or indirect "pile relief", as it allows for increased pile flexibility, which may lead to different effects on the superstructure as well. At the Kishwaukee Bridge, the top 10 ft of the abutment piles were encased in a soft bentonite slurry in order to provide pile relief. This particular method of pile relief was investigated on a limited basis as part of the prior parametric study portion of this project (LaFave et al. 2016). Results indicated that pile relief utilizing a bentonite slurry leads to reduced pile strains. Even though this type of pile relief increases pile deflections, the longer pile effective length leads to a reduction in pile bending moments. Modeling of the bentonite slurry at the Kishwaukee Bridge piles was included

in the FE model of the bridge, which resulted in better correlation of pile results between the FE model and field data, as will be further explained in Chapter 5.

Mechanically stabilized earth (MSE) walls can also be a likely source of indirect pile relief, as was the case at the UPRR Bridge. To analyze the effect of MSE walls on pile behavior, Han (2014) conducted full-scale testing of pipe piles located at different distances behind an MSE wall. Combined with results from previous work by Nelson (2013) and Price (2012), the study results indicated that the lateral resistance of piles decreases as the distance from the pile to the MSE wall decreases. The presence of the MSE wall results in a smaller amount of soil surrounding the pile, decreasing the foundation stiffness in the contraction direction. In order to account for the effect of the MSE wall, so called "p-multipliers" can be back-calculated to account for the reduced soil capacities. Results from Han (2014) combined with the previous results from Nelson (2013) and Price (2012) were utilized to create a p-multiplier curve to represent the relationship between p-multipliers and the spacing between a pile and MSE wall, as shown in

Figure 4. These p-multipliers allow for modifications to load-deflection curves in order to consider MSE wall effects in modeling. The effects of the MSE wall at UPRR were accounted for utilizing this method. The corresponding p-multiplier was calculated and implemented in the FE model, as further explained in Section 5.1. However, it should be noted that the results from Han, Nelson, and Price were from studies conducted on steel pipe piles. Parametric study results from LaFave et al. (2016) show that pipe piles and H-piles have similar behaviors until pipe piles reach yielding. Therefore, application of Han (2014) on bridges with H-piles may become less reliable above the pile yielding limit.

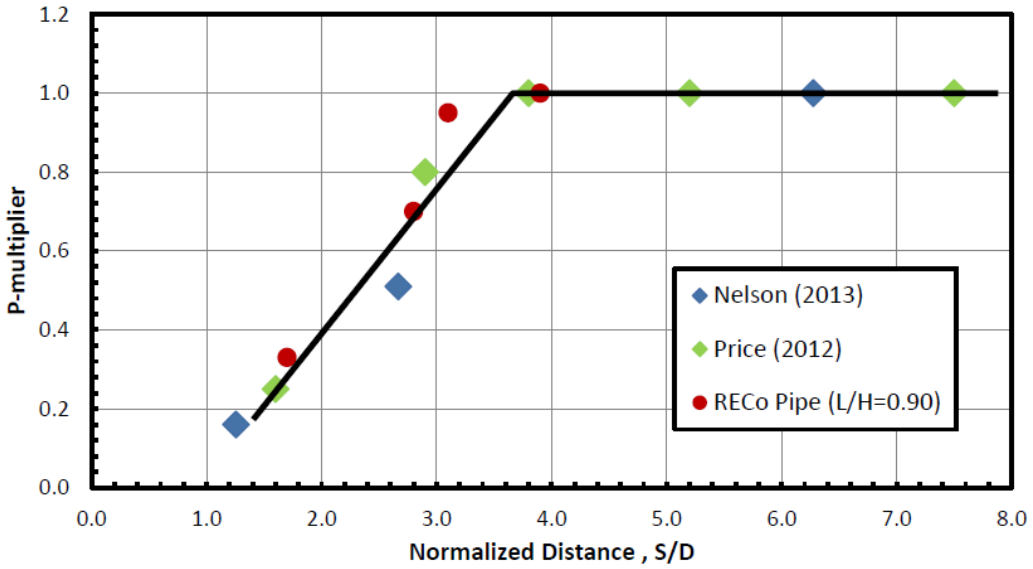

Figure 4. P-multiplier curves (Han 2014, Figure 6.8).

CHAPTER 3: SUMMARY OF PRIOR PARAMETRIC STUDY RESULTS

As previously mentioned, a parametric study was conducted earlier as part of this overall project, preceding the field monitoring of the UPRR and Kishwaukee Bridges. The goal of the parametric study was to investigate a broad range of parameters associated with superstructure behavior, in order to provide improved design recommendations. The field monitoring of the two IABs was implemented to complement those results and further investigate IAB structural behavior. As will be shown later, field monitoring results were compared to parametric study results to further analyze trends and corroborate previous parametric study findings. This chapter summarizes some of the main parametric study findings; further details can be found in LaFave et al. (2016).

A large suite of three-dimensional FE numerical models of IABs – including bridge superstructures, abutments, piers, and pile foundations – were developed in *SAP2000 v14* (CSI 2009) for the parametric study. Models were run using nonlinear analysis for various combinations of dead, thermal, and live loads. Based on AASHTO design provisions and communication with IDOT, a temperature change range of –80°F to +80°F was used. (This same modeling procedure and other modeling assumptions were implemented in the FE models of the instrumented bridges as well). The parametric study was divided into an analysis of primary and secondary parameters. The majority of the primary parameters revolved around bridge geometry and included abutment skew, pile size, number of spans, and span length, among others. For each model, all variables were set to their default values except for a parameter of interest.

The three main aspects of IAB structural behavior that were analyzed were bridge displacement at the deck level, pile strains, and girder stresses. Results from the primary parameter models demonstrated that IAB global movement is directly proportional to effective expansion length (EEL) and is typically around 90% of theoretical free expansion / contraction. The degree of abutment skew was also shown to affect global movement, amplifying transverse displacement in bridges with higher degrees of skew. Bridges with moderately-high degrees of skew (above approximately 35°) demonstrated non-symmetric movement of the bridge acute and obtuse corners, as opposed to the mostly symmetric movement observed in zero to low skew bridges. As expected, increased pile size led to a decrease in total pile strains, with peak pile strains observed at the acute corner pile. Peak pile strains also increased with increasing abutment skew and EEL.

Analysis of the girders found that their largest magnitude stresses were observed at the girder bottom flanges, with maximums at the abutment. Increased bridge skew was seen to decrease girder stresses resulting from strong-axis bending but increase girder stresses resulting from weak-axis bending.

The secondary parameters, which included end-span length, bridge width, backfill stiffness, different pile conditions, and abutment height, among others, were investigated on a limited basis. Results indicated that larger bridge widths only affected pile demands, by increasing pile strains as width increased (especially in higher skewed bridges). Stiffer backfill soils decreased pile strains but caused larger superstructure demands. Similarly, stiffer foundation soils increased pile strains and girder demands. Pile top relief, due to use of bentonite slurry around foundations piles, resulted in larger pile deflections yet decreased pile demands due to the increased pile effective length. Of the different pile conditions investigated, piles in weak-axis orientation were observed to be the preferred pile detail because they did not display any detrimental pile section stiffness loss after yielding.

Results from the parametric study allowed for the creation of design aids and improved design recommendations. The design aids included nonlinear regressions and pile charts similar to those in current used by IDOT. Overall, the results provided a fairly comprehensive understanding of both IAB substructure and superstructure behavior. These parametric study results have now been compared to field monitoring results, as will be shown in Chapter 6.

CHAPTER 4: MONITORING OF TWO ILLINOIS INTEGRAL ABUTMENT BRIDGES[1]

This chapter provides an overview of the bridge sites, instrumentation goals, and the field instrumentation and monitoring schemes used for the two (2) Illinois IABs that were instrumented and monitored as part of this project. Some related details about this part of the work may also be found elsewhere (Wright et al. 2015), which is co-authored by all the individuals who participated in the overall IAB field instrumentation and monitoring effort.

4.1 BRIDGE SITE DESCRIPTIONS

Two Illinois Tollway I-90 mainline IABs located in northern Illinois were chosen for instrumentation and field monitoring, the EB UPRR Bridge and EB Kishwaukee River Bridge. Table 1 summarizes the overall bridge geometry information for both bridges. The Eastbound Kishwaukee River Bridge is a four-span continuous bridge with span lengths of 125 ft, 152 ft, 152 ft, and 120 ft from east to west. The Kishwaukee Bridge is of particular interest as it is only a mere 1 ft short of the current 550 ft maximum permissible length for IDOT multi-span IABs. This bridge is also of interest because it employs HP14x117 piles, which is the largest pile size currently in service for IDOT IABs. Otherwise the Kishwaukee bridge geometry is standard, with a 30° abutment skew, approximately a 1.25 end-span to intermediate-span ratio, a 69 ft width, and a typical girder design. All deck, abutment, and approach slab dimensions conform to standard IDOT details. Construction of the Kishwaukee Bridge concluded in October of 2013.

1 *Chapter includes work co-authored by all the individuals who participated in the overall IAB field instrumentation and monitoring effort and previously published in Wright, B., J. LaFave, L. Fahnestock, M. Jarrett, J. Riddle, and J. S. Svatora (2015). "Field Monitoring of Skewed Integral Abutment Bridges," 2015 Joint Conference AESE/ANCRiSST, Entry 228.*

Bridge	Kishwaukee	UPRR
Spans	125’-152’-152’-120’ (West to East)	184.5’
Overall length	549’	184.5’
Width	69’-1/4”	69’-1”
Abutment skew	30°	42.5°
Number of girders	8	10
Girder size	Plate Girder: 60” Web	Plate Girder: 72” Web
Abutment piles	30 (15 each end)	38 (19 on each end)
Abutment pile size	HP14x117	HP14x89

Table 1. Bridge geometry information for the Kishwaukee and UPRR bridges.

The Eastbound UPRR Bridge is a single-span structure, with a length of 184.5 ft, which exceeds the current IDOT limit for a single-span IAB. The bridge is also of interest because it is only 2.5° below the current IDOT skew limit of 45°. The UPRR Bridge also utilizes MSE walls at each abutment, which are no longer permitted for use with IABs according to the latest IDOT Memo regarding design and construction of IABs (IDOT ABD Memo 12.3). Otherwise the UPRR Bridge geometry is relatively modest and/or is based on standard IDOT details. The bridge was built with stage construction: Stage 1 included approximately the southern one-third of the bridge, and Stage 1A included the remaining two-thirds of the bridge. The bridge was completed in April of 2014 after delays due to extreme cold winter weather.

4.2 INSTRUMENTATION GOALS

The project’s instrumentation goals were greatly based on specific requests of various parties at IDOT and the Illinois Tollway, as well as from the need to validate modeling assumptions utilized in the prior parametric study phase of this project and in the analytical IAB models associated with the instrumented bridges. Since the project mainly focuses on the behavior of IAB superstructures, most of the instrumentation effort was placed on the bridges’ superstructures, with limited additional instrumentation on the substructure, as summarized in Figure 5.

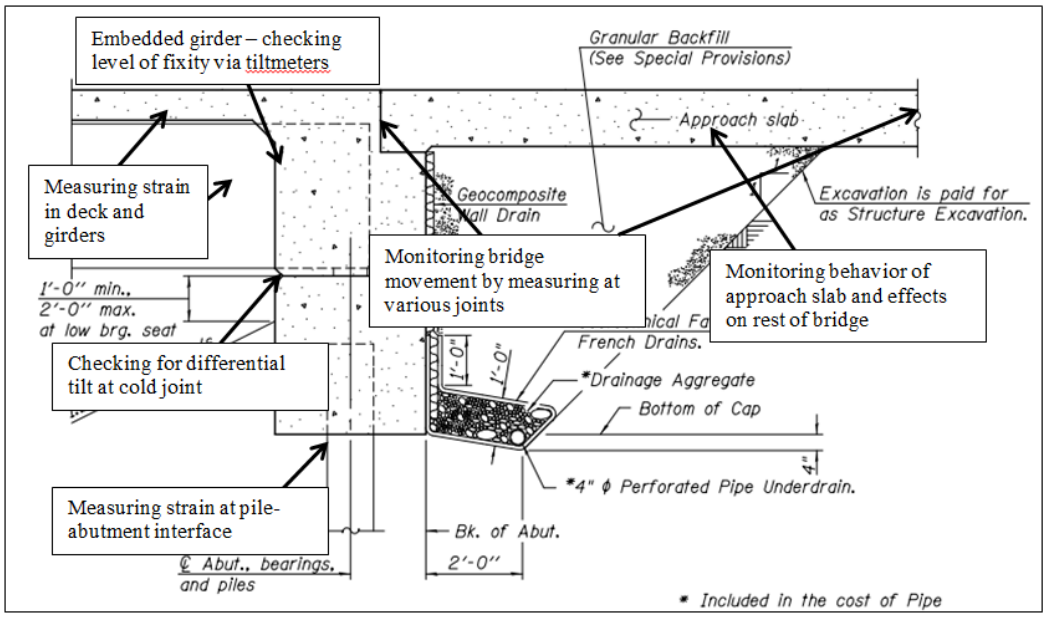

Figure 5. Schematic of project instrumentation objectives.

A large motivator of this project was the need for further understanding of IAB superstructure behavior. One concern for IAB superstructure behavior, which has scarcely been investigated to date, is the additional buildup of thermal stresses in the superstructure due to the integral abutment construction. To further investigate superstructure behavior, strain gages were installed at different girder cross sections throughout each bridge, with gages at different depths of the girder and embedded in the deck. Another aspect of interest is the global bridge displacement at the deck level caused by volumetric changes in the structure itself due to thermal and other loading effects. At the Kishwaukee Bridge, displacement transducers ("crackmeters") were placed at the approach slab – transition slab, approach slab – abutment, and pier – girder interfaces in order to measure global bridge movement. To complement those results, standard surveying of one abutment was also done on a limited basis to capture absolute abutment movement during extreme cold and extreme heat.

In order to validate previous modeling assumptions, it was important to include instrumentation to evaluate the rigidity at the abutment cold joint and girder-abutment interface. In the parametric study models and models of the instrumented bridges, both of these interfaces were assumed to be rigid connections. The cold joint between the integral abutment lower footing (pile cap) and upper diaphragm is typically heavily reinforced in hopes it will behave in a continuous, moment-resisting fashion. To evaluate this assumption, tiltmeters were installed above and below the joint to

measure any differential rotation that might occur. The girder to abutment connections are also assumed to be rigid since the girder is embedded into the abutment. Therefore, tiltmeters were also installed at the girder end to measure any differential rotation versus the abutment. This measurement of differential rotation directly corresponds to the level of fixity at this connection. Results from the tiltmeters allowed validation of these rigid connection assumptions and further investigation of IAB behavior.

Monitoring of approach slab behavior was also deemed important, especially as the parametric study found that approach slabs have minimal impact on IAB behavior and were therefore neglected in the analytical models. Therefore, a limited number of embedded strain gages were installed in one of the approach slabs at Kishwaukee in order to capture any build-up of stresses or axial force applied to the IAB superstructure. One possible result would be a build-up of axial force from frictional forces due to soil-concrete interaction on the bottom face of the approach slab. Finally, to obtain a comprehensive view of IAB behavior, some only limited focus was also placed on substructure behavior. Strain gages were attached to the flanges of the H-pile abutment foundations to gather strain data at the pile-abutment interface, which is where the maximum strain is known to occur.

4.3 DETAILED INSTRUMENTATION AND MONITORING SCHEME

In order to minimize costs and simplify the instrumentation scheme, the symmetry of the two bridges was utilized. Only the east half of the Kishwaukee Bridge and east abutment and foundations were instrumented, with the assumption that the west half would behave similarly. Similarly, only the west abutment and foundation of the UPRR Bridge were instrumented. All of the sensors and data acquisition equipment were procured from GEOKON, Inc., and are outlined in Table 2. Each sensor was equipped to monitor its respective strain, rotation, or displacement measurement along with a temperature measurement.

Sensor Name	Model Number	Range	Resolution	Accuracy
Arc-welded Strain Gage	4000	3000 με	1.0 με	+/- 0.5%
Spot-welded Strain Gage	4150	3000 με	0.4 με	+/- 0.5%
Embedded Strain Gage	4200	3000 με	1.0 με	+/- 0.5%
Tiltmeter	6350	+/- 10°	8 arc seconds	+/- 0.1%
Displacement Transducer ("Crackmeter")	4420	+/- 6"	0.025%	+/- 0.1%

Table 2. Sensors used at the monitored bridges.

4.3.1 Piles

Arc-welded strain gages were utilized to measure pile strains at both bridge sites. Three piles at the Kishwaukee east abutment and UPRR west abutment were instrumented. Two exterior piles – the pile nearest the obtuse corner and the pile 2nd-nearest to the acute corner – and a middle pile were chosen so as to represent the south, middle, and north portions of each bridge. This would allow for comparison of pile strains at or near both the acute and obtuse corners of each bridge. Two different instrumentation configurations were planned – configuration A, with a total of eight (8) gages, and configuration B, with a total of four (4) gages, as shown in Figure 6. Configuration A, planned for the exterior piles, has two sets of four (4) gages – one set at the pile cap boundary and the other 14 inches below that. Configuration B, planned for the middle pile, has only the top set of four (4) gages located at the pile cap boundary. The gages are located at the quarter points of each pile flange, as shown in Figure 7. This configuration would allow for calculation of axial force, strong-axis, and weak-axis moment of the piles utilizing the different pile data. It should be noted that during construction the south exterior pile and the middle pile at Kishwaukee were switched. Therefore, the north exterior and middle pile at Kishwaukee have configuration A of pile strain gages.

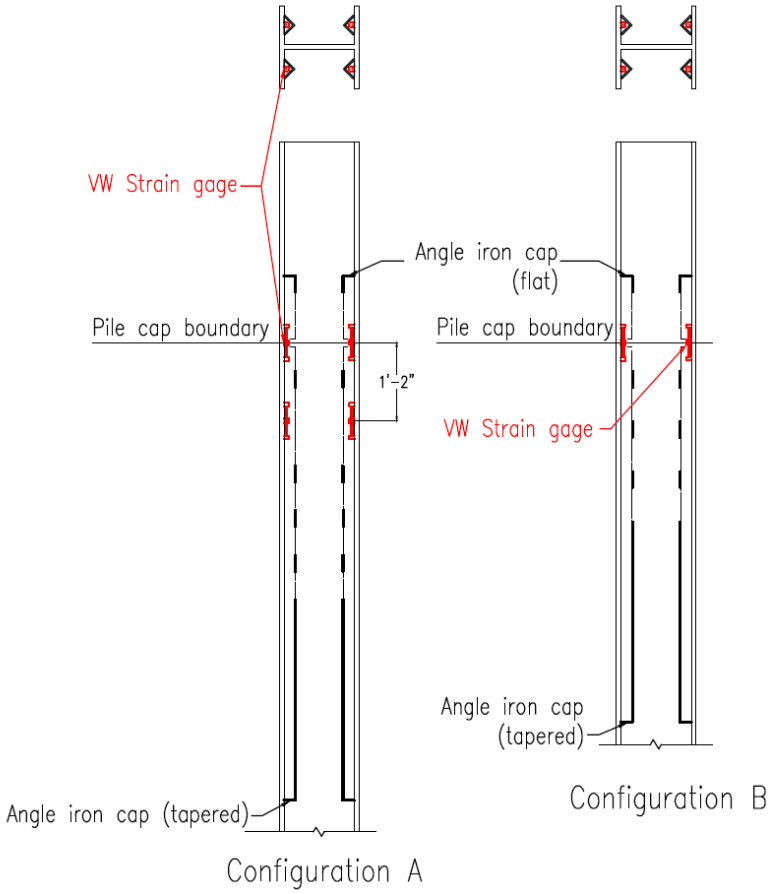

Figure 6. Pile instrumentation schematics.

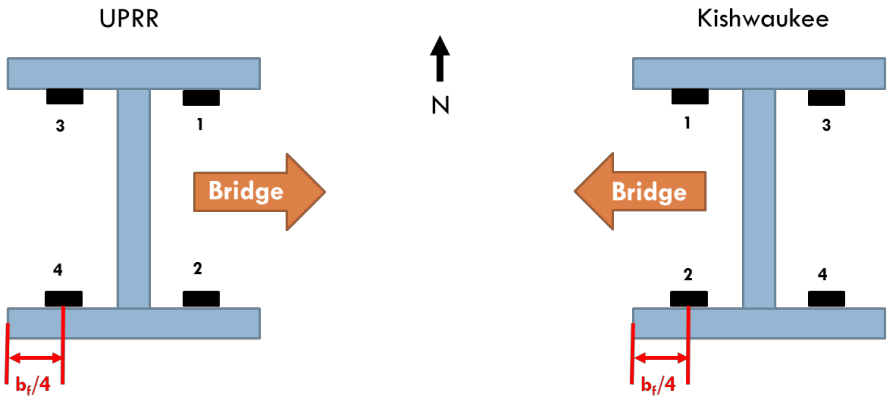

Figure 7. Schematic of pile strain gage locations.

A steel angle was installed to cover and protect the pile gages since they were instrumented prior to being placed in the field. The piles at Kishwaukee would be driven into the ground and thus an additional tapered end-cap was installed to protect the angles from being dislodged during the driving process. The arc-welded gages were attached using two steel mounting blocks and set

screws, as shown in Figure 8. The coil housing was secured to the gage using a hose clamp, and the wires exited the protective steel angle through a notch, which was later sealed with spray foam insulation.

Figure 8. Arc-welded pile strain gage installation.

4.3.2 Girders

Spot-welded strain gages were utilized to monitor girder strains at different cross sections along the three girders corresponding to the instrumented piles on each bridge. Several different cross sections at each bridge were instrumented with strain gages placed on the top flange, bottom flange, and mid-height of the girder web, as shown in Figure 9 through Figure 11. Similar to the piles, the spot-welded girder gages were attached to the girders at the steel fabricators before being shipped to the site. A semi-circle cover plate was attached over each gage as shown in Figure 12 to protect it from damage during construction and from general elemental exposure.

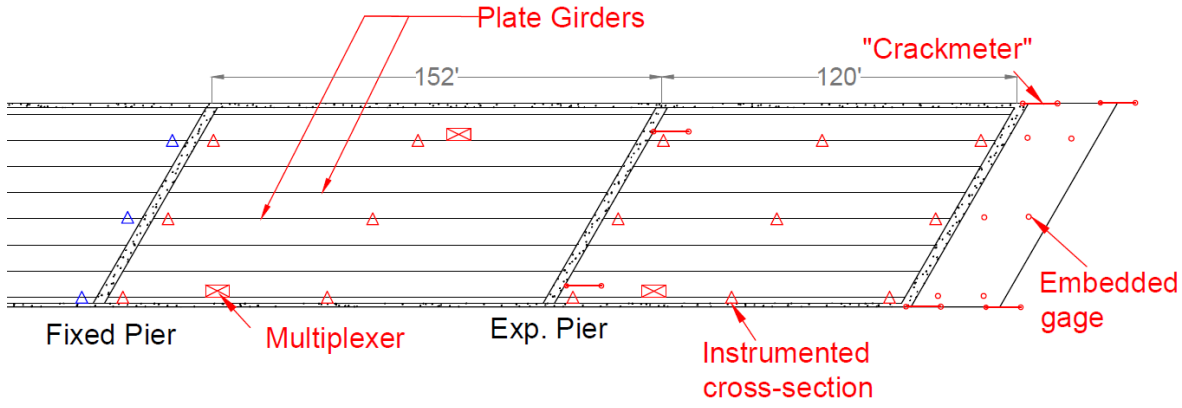

Figure 9. Plan view of instrumentation scheme for Kishwaukee.

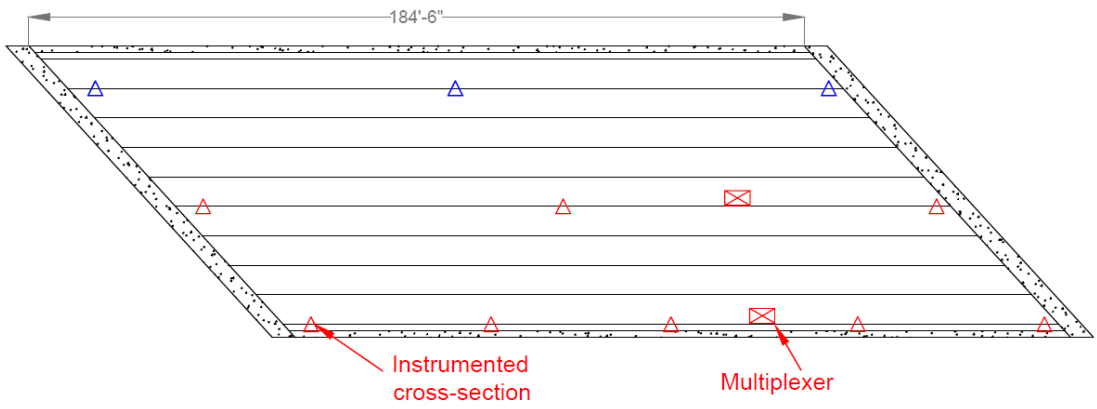

Figure 10. Plan view of instrumentation scheme for UPRR.

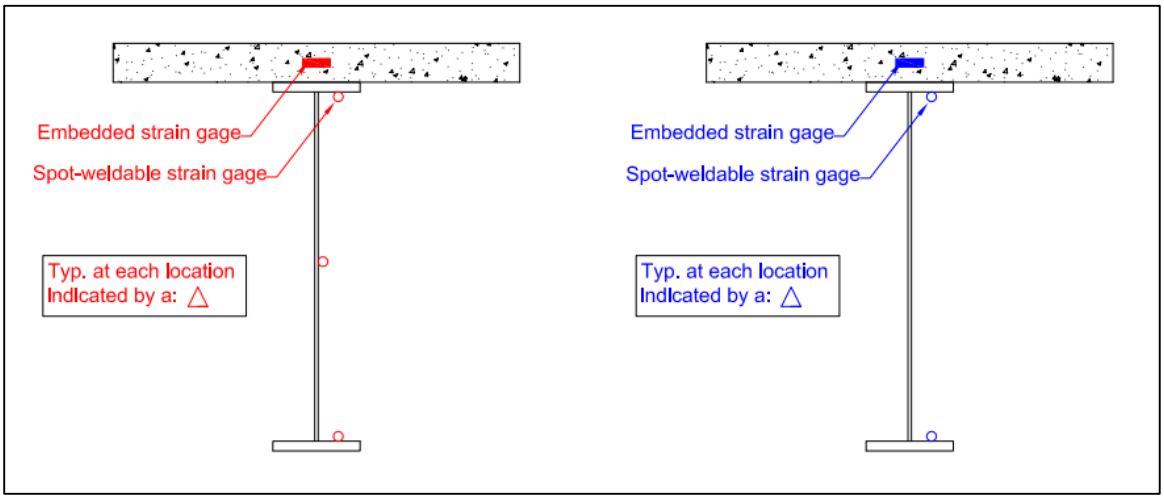

Figure 11. Instrumentation schematic for superstructure cross sections.

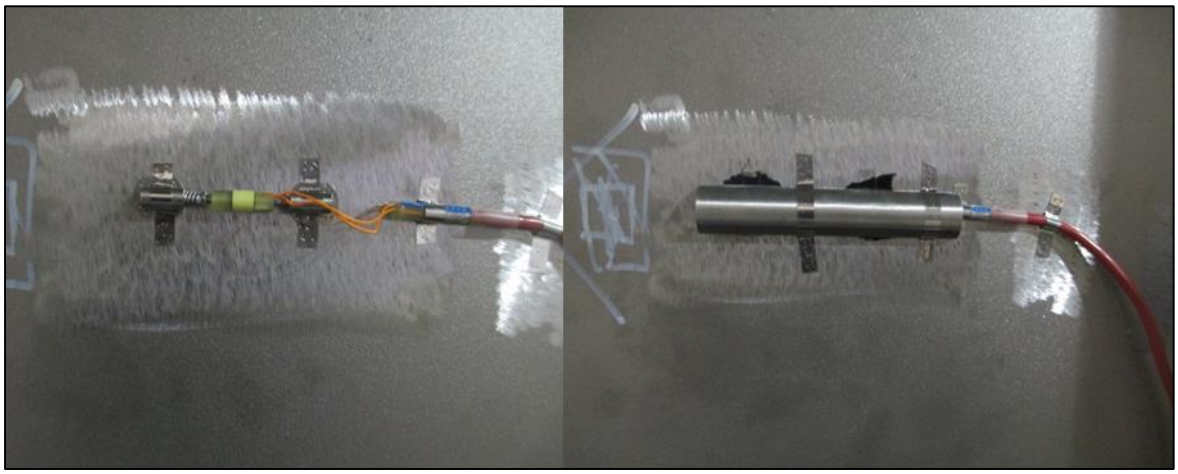

Figure 12. Spot-welded girder strain gage without and with its cover plate.

4.3.3 Deck and Approach Slab

Embedded strain gages were used to instrument the decks of both bridges. The strain gages were placed in the deck at the same location as the instrumented girder cross sections. Additionally, six embedded strain gages were installed in the east approach slab at Kishwaukee. Three (3) longitudinal lines, lining up with the instrumented girder lines, were instrumented with two (2) embedded strain gages along each line. The embedded strain gages in both the deck and approach slab were tied off to the steel reinforcement with wooden blocks so as to only measure the concrete strain, as shown in Figure 13. Coil housing was connected to the gage, with the wiring running along rebar and through the forms down to multiplexers attached to the girders.

Figure 13. Approach slab embedded strain gage.

4.3.4 Tiltmeters

Tiltmeters were placed at the ends of the instrumented girders and corresponding abutment locations in order to evaluate the rigidity of the cold joint and girder-abutment interface. The tiltmeters can only measure rotation about one axis, and thus were oriented to measure rotation in the longitudinal direction. The tiltmeters on the abutment were placed above and below the abutment cold joint as shown in Figure 14 and Figure 15. At the north and south abutment ends, tiltmeters were placed on the abutment above and below the cold joint and also on the girder end. In the middle of the abutment at Kishwaukee, tiltmeters were only placed on the abutment above the cold joint and on the girder end. In the middle of the abutment at UPRR, a tiltmeter was only placed above the cold joint of the abutment. The tiltmeters were attached to the steel girder using brackets or anchored to the concrete abutment, as shown in Figure 16. The tiltmeters are flush with

the abutment face, and thus an offset equal to the abutment skew is used when analyzing the field data, to account for the fact that the abutment and girder rotation measurements are not parallel to one another.

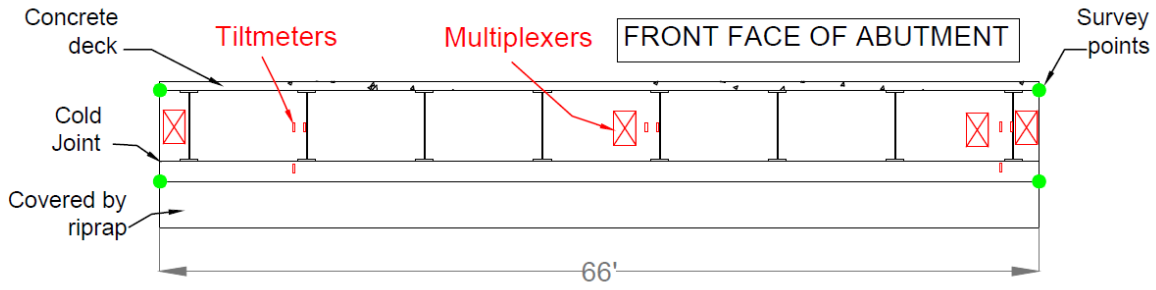

Figure 14. Elevation of east abutment at Kishwaukee.

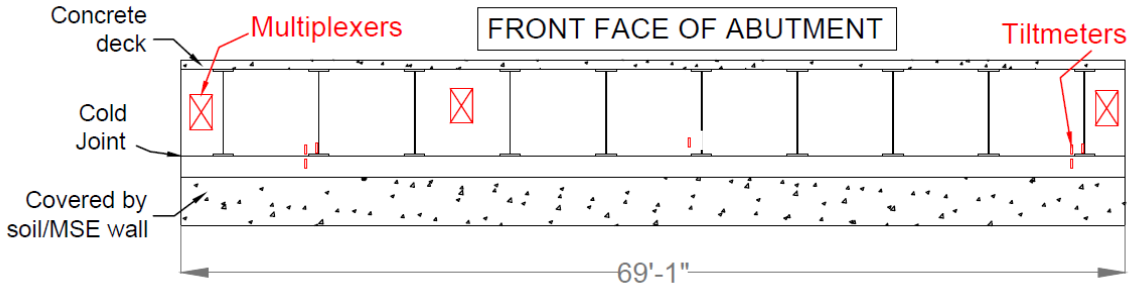

Figure 15. Elevation of west abutment at UPRR.

Figure 16. Tiltmeter installation at Kishwaukee on the north side (left) and middle (right) of abutment.

4.3.5 Displacement Transducers ("Crackmeters")

Displacement transducers or "crackmeters" were utilized to monitor the overall bridge movement of the Kishwuakee Bridge. Crackmeters were placed at the girder – pier, abutment – approach slab, and approach slab – transition slab interfaces at the north and south sides of the east half of the Kishwaukee Bridge. The largest available crackmeters, which have a range of +/- 6 in., were used to ensure an ability to measure the expansion joint displacements at the approach slab – transition slab interface. The approach slab crackmeters were anchored into the concrete utilizing small spacers and groutable anchors, as shown in Figure 17. At the girder – pier interface, the crackmeters were installed using various brackets in order to bolt one end to the cross-frame connection plate and then anchor the other end to the concrete pier. It should be noted that since these gages are anchored to structures that move due to thermal effects, the measurements provided are all relative displacements.

Figure 17. Crackmeter installed at approach slab – transition slab interface.

4.3.6 Surveying

To supplement the measurements from the crackmeters, surveying of the Kishwaukee east abutment was conducted in September 2014 and February 2015 at two points on both the north and south ends of the abutment. These survey points were determined to roughly align with the top and bottom of the girders, as indicated in Figure 14 and Figure 18.

Figure 18. Kishwaukee survey locations.

4.3.7 Data Acquisition

To facilitate consistent data collection, a remote data acquisition system was set up at both bridge site locations. A GEOKON Micro-1000 Datalogger was used at each site to collect the data. A cellular modem was placed at each site to allow for remote data collection. Since there was no direct access to power at either site, a 130 W solar panel and 2-110Ah batteries in parallel were installed at each site as a power source for the data acquisition system. To allow for the collection of data from a large number of gages, several multiplexers were placed throughout each bridge site to be used as junction boxes. A maximum of 16 instruments can connect to each multiplexer, which then in turn connect to the central Datalogger at each site. The multiplexers were mounted to the steel girders or the face of the concrete abutment.

Data collection from the Kishwaukee Bridge began on May 24, 2014 and continued for two years until May 26, 2016. At UPRR, data collection began on June 18, 2014 and ended on September 10, 2015. (Data collection at both bridges stopped due to issues connecting remotely to the datalogger and transferring data.) The sensors installed on the Kishwaukee Bridge were sampled every 15 minutes until March 2015. From then on, the sampling rate was modified to collect data every 5 minutes. For the UPRR Bridge, sensors were always sampled every 15 minutes. This interval allowed for suitable analysis of thermal load effects, however it only provides limited insight into dynamic or live loading effects. For data processing, a macro was created to save all the data to a field data Excel Workbook, after which MATLAB was used for data analysis and processing.

CHAPTER 5: FINITE ELEMENT MODELING OF INSTRUMENTED BRIDGES[2]

A finite element (FE) model was created for each of the instrumented bridges. These models were used in part to evaluate the results from the field monitoring investigation, as well as to expand more generally upon the understanding of IAB behavior. The same modeling assumptions and procedure used to create the parametric study models were implemented for the models of the instrumented bridges. This chapter provides a brief overview of the different modeling assumptions and procedures; further details can be found in LaFave et al. (2016), which is co-authored by all the individuals who participated in the overall IAB analytical model development effort.

5.1 MODELING ASSUMPTIONS AND PROCEDURE

The FE models of the instrumented bridges were created utilizing the structural analysis software *SAP2000 v14* (CSI 2009). Both frame and shell elements in *SAP2000* were used to model the bridges structural components, as shown in Figure 19. The bridge deck and abutment were modeled using thin- and thick-shell elements, respectively. It was assumed that minimal cracking was to occur under service loading and therefore the shell elements were modeled as linear elastic without steel reinforcement. The bridge girders were created using frame elements, which were made composite with the deck. The insertion-point method (CSI 2013) was employed to create the composite section. As in the parametric study models, the girder-to-abutment connections were modeled as fully rigid since the girder is embedded into the abutment. A rigid link connecting the girder end frame element to the corresponding abutment shell element simulated the rigid connection. The abutment cold joint was also modeled as a rigid connection.

---

2 Figure 19 adapted from and results developed with contributions from the co-authors of LaFave, James M., L. A. Fahnestock, B. A. Wright, J. K. Riddle, M. W. Jarrett, J. S. Svatora, H. An, and G. Brambila. (2016). Integral Abutment Bridges Under Thermal Loading: Numerical Simulations and Parametric Study. A report of the findings of ICT-R27-115. Illinois Center for Transportation Series No. 16-015. Research Report No. FHWA-ICT-16-014. Illinois Center for Transportation, Rantoul, IL.

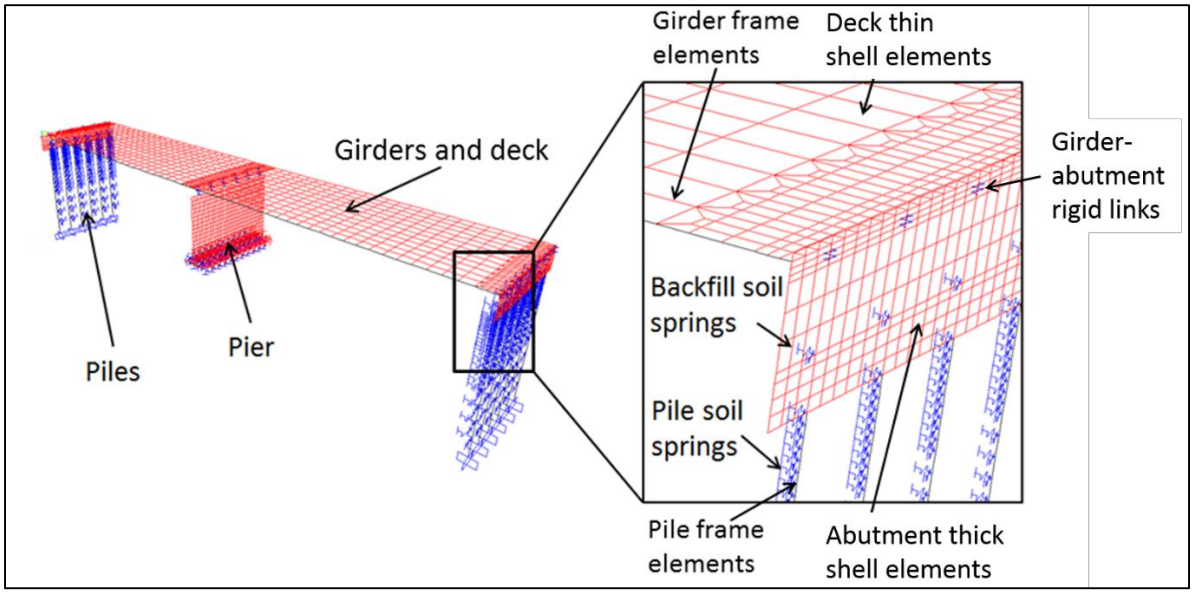

Figure 19. Typical finite-element model of an IAB (adapted from LaFave et al. 2016).

Modeling of the bridge piles was more intricate in order to capture the complete behavior of the piles even after yielding. 6-inch-long frame elements were used to model the piles, along with fiber section hinges applied to the top 5 feet of each pile to account for nonlinear behavior in this critical region. To facilitate post-processing, only one fiber hinge was assigned at the middle of each frame element and occupies the entire element length. This method made it possible to automatically calculate the hinge behavior analyzing nodal displacements and forces in MATLAB. Similar to the girders, the pile-abutment connection was modeled as rigid due to the 2 feet of pile embedment into the abutment at both bridges. The rigid connection was created by constraining the degrees of freedom of the section of the pile embedded in the abutment to those of the shell elements representing the bottom of the abutment.

For the mutli-span Kishwaukee Bridge, the three piers were also included in the model. The middle pier has a fixed bearing, while the other intermediate piers have expansion bearings. The wall pier component of the middle pier was modeled using thick-shell elements. Below the wall pier footing (pile cap), the piles and associated soil are represented using a linear 6-degree-of-freedom (DOF) nodal spring. Utilizing the software *LPILE* (Ensoft 2005), the spring stiffness was determined by applying a small deformation at the pile top with the appropriate boundary conditions in each degree of freedom. The fixed bearings that connect the pier to the superstructure were modeled as

rigid links. The intermediate piers with expansion elastomeric bearings were simply modeled as rollers.

The backfill and pile foundation soil properties at both bridge sites were also accounted for in the models by utilizing springs. The abutment backfill was modeled as single springs at the soil-pressure resultant locations across the width of the abutment. The springs have only two orthogonal components, aligned with the abutment axes. The component parallel to the abutment skew represents the soil friction parallel to the abutment surface. The component normal to the abutment represents the backfill soil pressure. Similarly, properties of the foundation soil surrounding the piles at each site were incorporated utilizing nonlinear springs. Each spring has two orthogonal components, which are aligned with the bridge directions, thus excluding vertical soil friction effects. The springs were placed every 6 in. for the top 5 ft of each pile, every 1 ft for the following 5 ft, every 2 ft for the subsequent 10 ft, and then every 20 ft for the remaining depth of the pile after that. The specific boring log data from each site was utilized to determine the inputs for the *LPILE* software. *LPILE* was then utilized to generate the lateral load-displacement (P-y) curves for each soil spring. For the Kishwaukee Bridge, the P-y curves obtained from *LPILE* were then modified to take into account pile relief due to the bentonite slurry surrounding the top 10 ft of the piles, as shown in Figure 20.

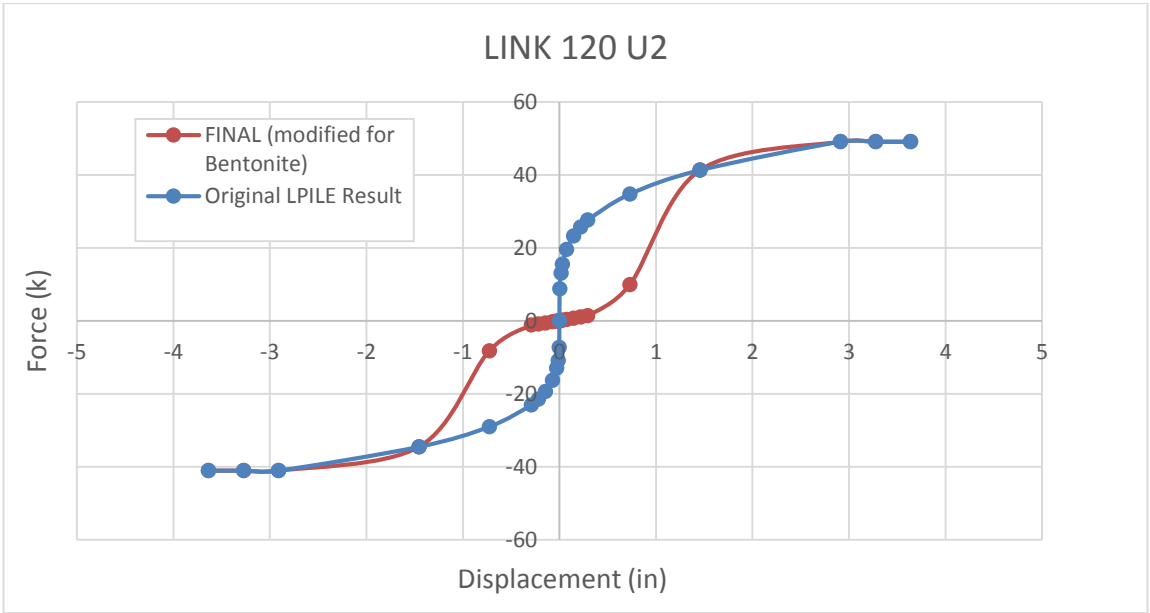

Figure 20. Kishwaukee P-y curve for soil spring in the longitudinal bridge direction at 10-ft depth.

At the UPRR Bridge, there is more uncertainty regarding foundation soil modeling because the sandy soil and MSE wall effects are much more difficult to model accurately. An initial model of UPRR was created using the given boring log data to create the soil spring P-y curves, but with no consideration of the MSE wall. Results from the model implementing those original P-y curves demonstrated trends fairly consistent with those seen in the field; however, the model greatly overestimated the strains seen in the field measurements, as depicted in Figure 21. In order to improve the UPRR model, the field data was further analyzed and different possible explanations for the differences between the model and field results explored, including pile-head fixity, MSE wall effects, and abutment rotation. The different explanations and possible methods of modeling the site conditions were explored, and results compared to the measured field pile strains. The most promising results came from using a so-called "P-multiplier" to consider the effect of the MSE wall.

As mentioned in Section 2.3, this P-multiplier has been explored by Han and found to be an appropriate method to consider MSE wall effects (2014). The study found that the MSE wall affects the effective foundation soil stiffness, resulting in a pile closer to an MSE wall requiring less force to create a certain displacement. This indirect "pile relief" is modeled utilizing a P-multiplier, which is determined based on the pile diameter and distance to the MSE wall. The corresponding P-multiplier of 0.42 for the UPRR piles was implemented to modify the P-y curves of the longitudinal component of the soil springs along the top 20 ft of the piles, only in the contraction direction, as shown in Figure 22. The P-multiplier was only applied to the top 20 ft of soil springs since that is roughly the depth the MSE wall reaches. Results from the updated model incorporating this P-multiplier demonstrated much better correlation with field pile strain results, as shown in Figure 21. This updated model was the final model utilized for comparison and analysis of the UPRR field data used in Chapter 6.

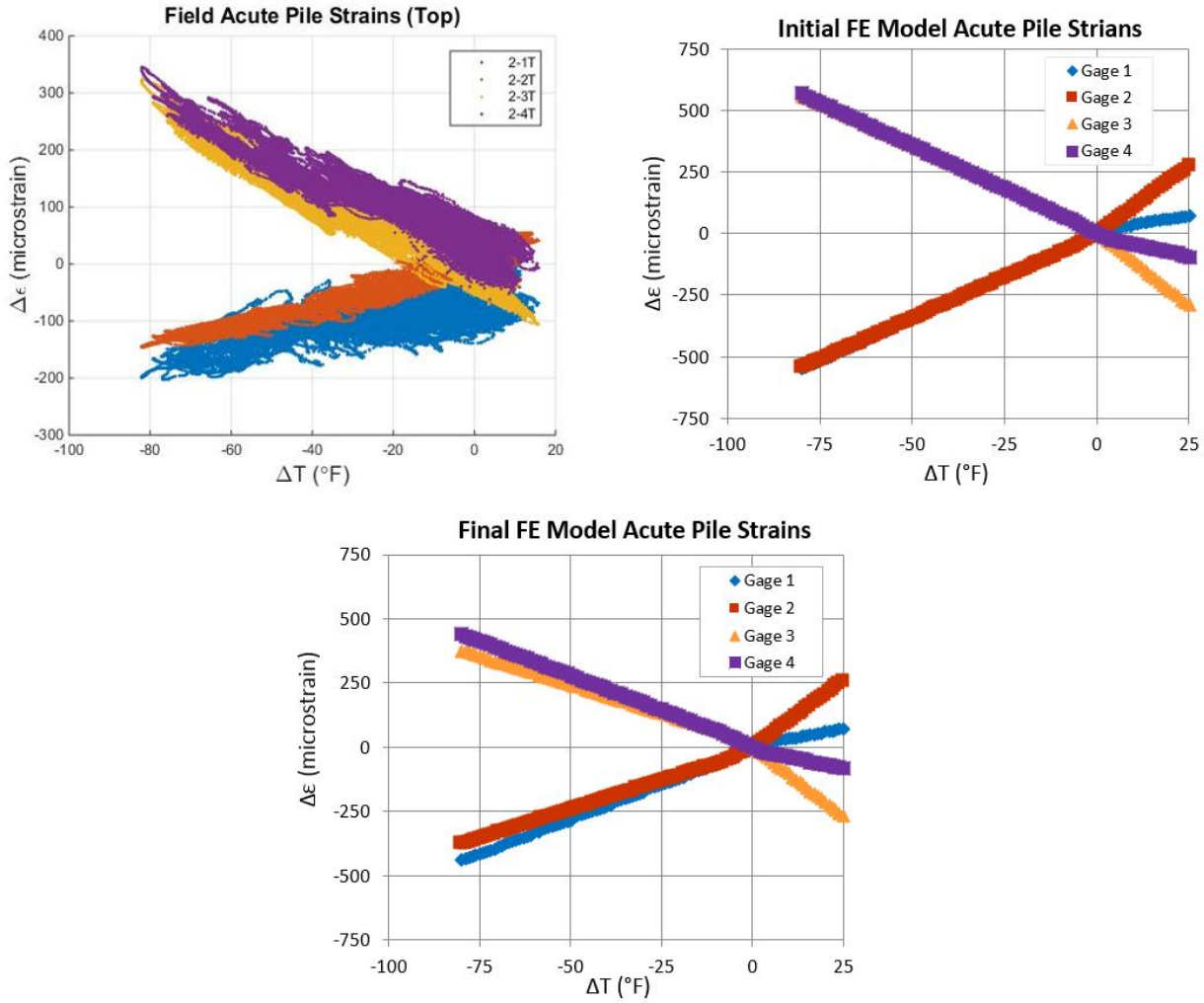

Figure 21. Comparison of UPRR field (top left), initial FE model (top right), and final FE model (bottom) acute pile strains.

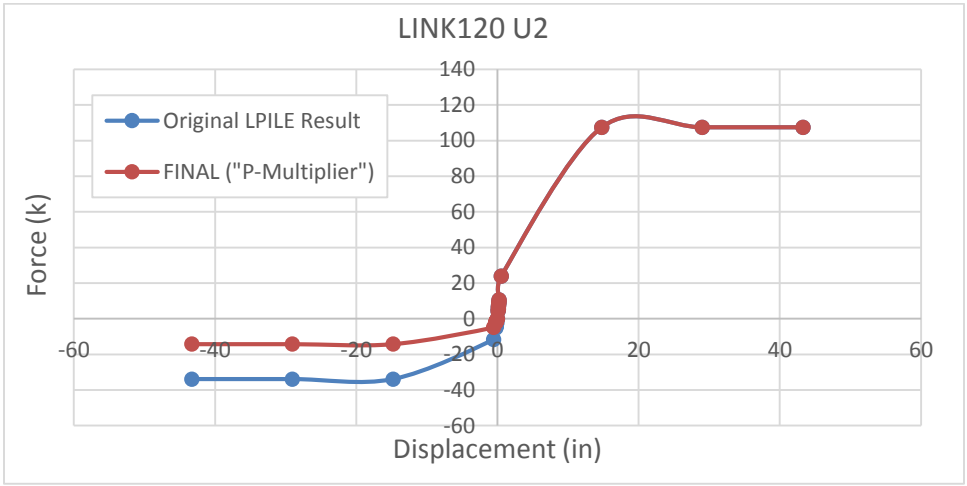

Figure 22. UPRR P-y curve for soil spring in the longitudinal bridge direction at 10-ft depth.

Several other modeling simplifications that were explored and implemented in the parametric study models were also implemented into these instrumented bridge models. The inclusion of wingwalls was considered but finally excluded based on previous research at Minnesota (Huang et al. 2004) and at Illinois (Olson et al. 2012), which concluded that wingwalls should only have a minor effect on IAB behavior. The effect of approach slabs on bridge behavior was analyzed as part of the parametric study modeling and finally excluded, as results showed little to no effect. Several parametric study models were also created to evaluate the effects of including girder camber. Results from models including girder camber demonstrated that the girder forces, pile forces, and superstructure and abutment-pile displacement results were very close to the corresponding models without girder camber. Therefore, girder camber was not explicitly included in the modeling process. The effect of including cross-frames was also explored with two bridge models, one with angle cross-frames and one with horizontal channel diaphragms. Bridge behavior was largely unaffected, and thus cross-frames were not considered in the models.

5.2 LOAD CASES AND ANALYSIS

Even though the main focus of the project is to analyze IAB behavior under thermal loading, the instrumented bridge models were run for applied dead load, thermal load, and live load conditions. Since the main objective of the project was to investigate bridge behavior under service conditions, the applied loads were all unfactored. Due to the staged construction, the dead load scenario was modeled using a nonlinear staged construction analysis with three different stages. Both the thermal and live load cases were modeled using nonlinear static analysis. For the thermal load case, a range of +80 to -80 °F *change* in temperature was applied uniformly to the girder frame elements and deck shell elements. Applying a temperature gradient rather than a uniform temperature was explored as part of the parametric study modeling. Since no drastic differences were found between the two methods, a uniform temperature was applied to simplify the modeling process and analysis. Coefficients of thermal expansion of 5.5×10^{-6}/°F and 6.5×10^{-6}/°F were used for concrete and steel, respectively. For live loading, the standard AASHTO HL-93 truck load was used. A uniform load was applied on the entire bridge to represent the design lane load, along with an additional equivalent uniform load placed at the center of one end-span. Since the main focus of this project is to explore behavior under thermal loading and the field data mainly represents thermal effects, analysis of the model data was primarily focused on the pure positive

and pure negative thermal load cases. The pure thermal load cases do not include dead load effects and are calculated utilizing results from the dead and thermal load cases, as shown in Table 3. The FE model data presented from this point forward is for the pure thermal positive and negative load cases, unless specifically noted otherwise.

Method	Actual Loading	Shorthand
Analyzed in SAP2000	Dead: Staged Construction	Dead Staged
	Dead + HL-93 Live	HL-93
	Dead + Positive Thermal	Positive Thermal
	Dead + Negative Thermal	Negative Thermal
	Dead + Positive Thermal + HL-93 Live	HL-93 Positive Thermal
	Dead + Negative Thermal + HL-93 Live	HL-93 Negative Thermal
Computed from results	Dead + Positive Thermal—Dead Staged	Pure Positive Thermal
	Dead + Negative Thermal—Dead Staged	Pure Negative Thermal

Table 3. Load Cases.

CHAPTER 6: COMPARISON OF FINITE ELEMENT MODEL RESULTS AND IAB FIELD DATA

6.1 FIELD DATA INITIALIZATION

In order to have a uniform point of comparison, an "initial reading" for each of the gages had to be decided upon. Initial readings, right after installation, were only taken for the girder spot-welded strain gages; however, utilizing these initial readings would not be indicative of the girder condition upon bridge completion. Therefore, to be consistent for all gages, the data was initialized with the first collected data point for each gage. This would thus be most indicative of the bridge condition after it became integral, and hence it is assumed that this already incorporates the dead load contribution. The ensuing calculated measurements are then due only to thermal changes, perhaps along with some modest live-load and/or other time-dependent effects. It should be noted that data collection began in the summer and therefore the first data points were taken at relatively warm temperatures, so most of the field results represent net thermal contraction.

6.2 FIELD DATA AVERAGE SUPERSTRUCTURE TEMPERATURE

Since the main focus of the study is on thermal effects, a definition of the average bridge superstructure temperature had to be determined. Temperature readings from the gages on all the different bridge components were analyzed and then compared to ambient air temperature data from a location near each bridge. It was found that the girder strain gages best represented the air temperature. Focusing on only the girder gages, an average of the strain values at a specific girder depth (e.g., top flange, web, bottom flange) along each instrumented girder was taken. Comparing the average temperature readings along each girder, it was found that the readings from the middle girder were in a narrower range, while the exterior girder readings displayed larger temperature differences. Therefore, it was determined that averaging the temperature readings of all the strain gages on the middle girder would provide the best indicator of the average superstructure temperature. This same definition was utilized for both bridges; however, for the UPRR Bridge, readings from the gages at the instrumented cross section closest to the west abutment on the middle girder were not included because their temperature trends were inconsistent with the trends for the rest of the bridge. This definition was used to analyze data from all of the gages except the approach slab strain gages, as further explained in Section 6.3.2.

To validate this definition of average superstructure temperature, the data was compared with that from a weather station at the nearest airport to each bridge site, which were Rockford International Airport (10 miles from the Kishwaukee Bridge) and DuPage Airport (15 miles from the UPRR Bridge). The calculated field average superstructure temperature of each bridge matches the temperatures reported from the corresponding airport weather data fairly well throughout the seasons, with the best correlation during warmer seasons. However, the average superstructure temperature lags slightly behind the weather station temperature. The average superstructure temperature was initialized in the same fashion as the other gage measurements, where the initial data points were 75 °F and 73 °F for Kishwaukee and UPRR, respectively. Thus, the majority of the reported field data represents net thermal contraction.

6.3 GLOBAL BRIDGE MOVEMENT

6.3.1 Crackmeter Results

Observing IAB deck displacement and overall bridge movement was a key aspect of this research project. Global bridge movement of only the Kishwaukee Bridge was monitored with the use of crackmeters, which measure relative displacement. Results from the crackmeters demonstrate a clear relationship with change in temperature, as expected. Crackmeter results appear in a band, in part due to any influence of live-load and/or other time-dependent effects. Even so, most of the crackmeter data demonstrates a clear linear trend against change in temperature as seen in Figure 23. The largest magnitude of displacement is observed at the approach slab – transition slab interface. This finding is as expected because it is the location of the expansion joint, which accommodates bridge expansion and contraction. Data from this interface at both the north and south bridge faces display a shift after the first full year of data collection, when the bridge appears to have overcome some resistance and the joint closed beyond its original gap width, setting up a new “permanent” displacement. This shift could in part be explained by possible backfill soil compaction occurring after the first bridge expansion cycle, thus permitting for further bridge expansion and closing of the expansion joint during the following expansion cycle.

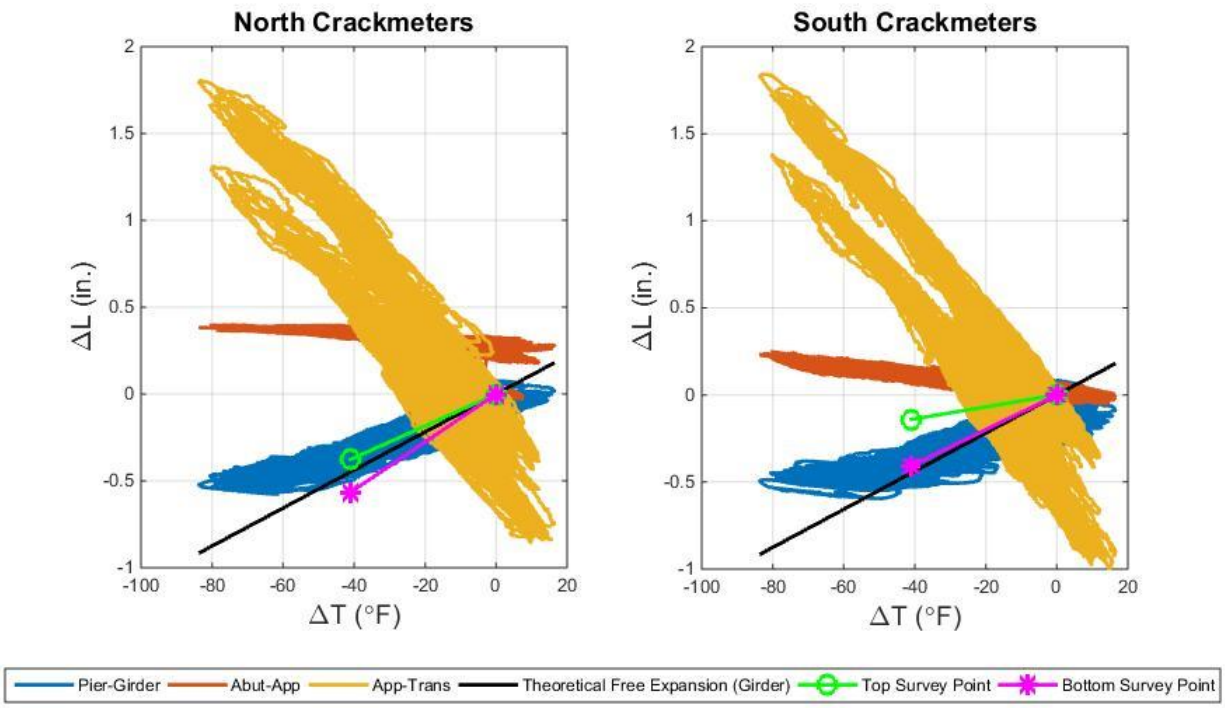

Figure 23. Kishwaukee crackmeter displacements.

The approach slab – abutment crackmeter data also follows a linear trend, yet with a much shallower slope than the approach slab – transition slab data. This limited amount of displacement observed at the approach slab – abutment interface is as expected due to reinforcing steel continuity across this construction joint. There is a slight jump in the north approach slab – abutment curve, which is likely due to the removal of construction equipment on and/or near the approach slab. Looking at the pier – girder crackmeter displacements, Figure 23 shows that the displacements are lower than those calculated for theoretical free expansion/contraction (using a coefficient of thermal expansion of 6 x 10^{-6} in./in./°F for the 152-ft span of composite plate girder and concrete deck from the middle of the bridge out to this pier). This finding supports results from the parametric study which concluded that longitudinal bridge movements at the deck level only reach about 90% of theoretical free thermal expansion/contraction (LaFave et al. 2016). The pier – girder curves on both the north and south faces also appear to shallow out after reaching a change in temperature greater than -50°F. This trend could likely be due to interaction with the expansion bearing at such cold temperatures.

6.3.2 Approach Slab Results

Results from the Kishwaukee approach slab embedded strain gages were utilized to better understand approach slab behavior and to help calculate bridge abutment movement. During analysis of the approach slab gages' temperature readings, it was noted that the average temperature of the approach slab differed from the calculated average bridge superstructure temperature (from Section 6.2) by an average of ± 5 °F, and sometimes up to 22 °F, as can be seen in Figure 24. Minimal differences were observed between the temperature readings of the different gages throughout the approach slab. Therefore, the average temperature reading from the approach slab gages was utilized as the approach slab temperature for subsequent analysis of the approach-slab data (i.e., for gage-temperature correction).

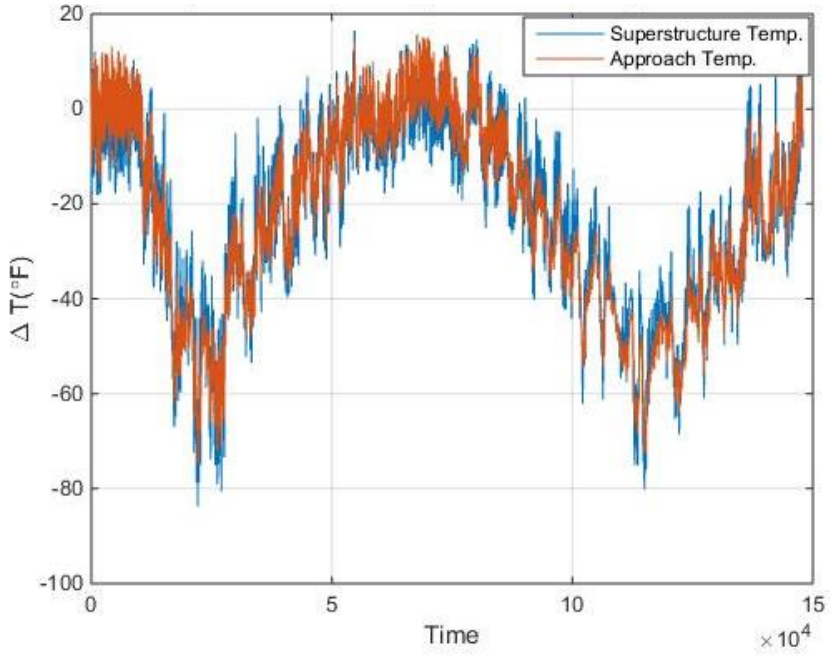

Figure 24. Comparison of average superstructure temperature and average approach slab temperature over time (Kishwaukee).

Readings from each approach-slab strain gage trend well over time with the average approach-slab temperature, as shown in Figure 25. However, since the approach slab gages are embedded in concrete, the strain readings need to be corrected to account for the temperature effects on the gage due to the difference in coefficient of thermal expansion of the steel vibrating wire of the gage and of the concrete the gage is embedded in. Accounting for this correction then gives the actual strain of the concrete member (i.e., the change in unit length that a dial gage attached to the surface would measure), which is given by:

$$\Delta\varepsilon_{actual} = \Delta\varepsilon_{measured} + \Delta T_{Approach\ Slab} \times \alpha_{gage\ steel} \quad (1)$$

where $\Delta\varepsilon_{measured}$ is the change in strain directly reported from the readout/datalogger in microstrain, and $\alpha_{\text{gage steel}}$ is the coefficient of thermal expansion of steel (6.78 microstrain/°F for a model 4200 embedded strain gage).

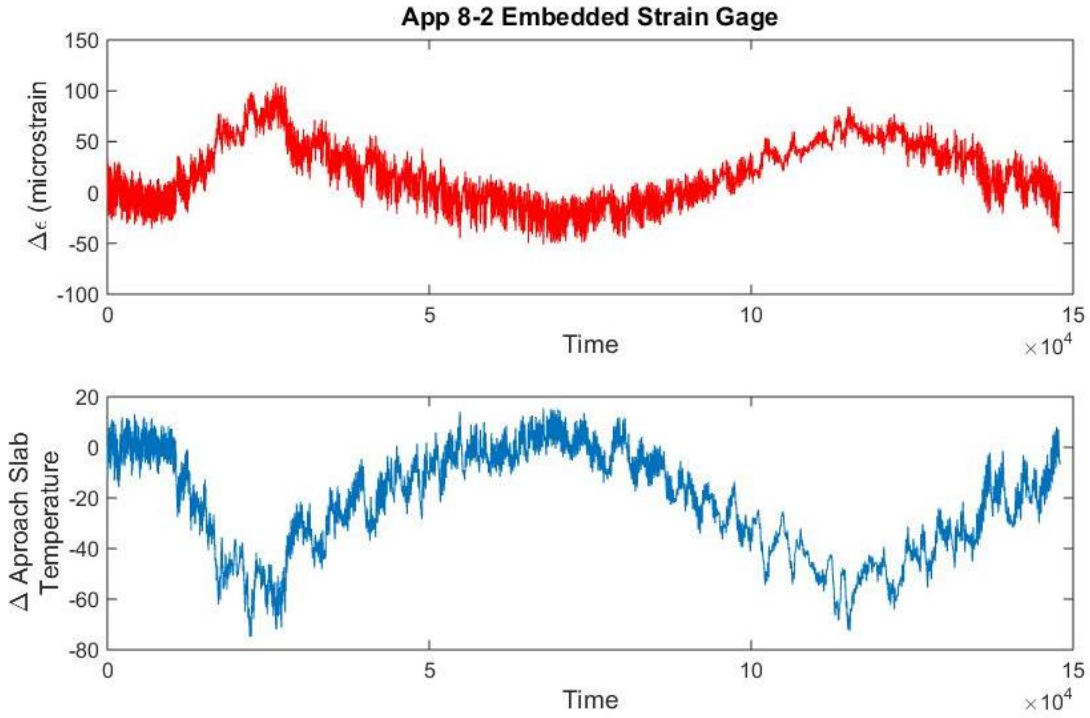

Figure 25. Approach slab 8-2 gage strain and average approach slab temperature vs. time (Kishwaukee).

Assuming that the approach slab remains in the elastic regime, the calculated actual approach slab strains could then be utilized to estimate the approach slab change in length. The average actual strain along each longitudinal instrumented line was calculated, using equation 1, and then multiplied by the approach slab's total length (30 ft) to obtain a change in length along each instrumented line. Figure 26 shows that the north and south sides of the approach slab had very similar change in length. Overall, the approach slab contracts (designated by a negative change in length) during negative changes in temperature. Therefore, it was concluded that the approach slab goes through its own cycles of thermal expansion and contraction, which are not entirely inhibited by the bridge's expansion and contraction due to the relative freedom of movement provided by the expansion joint. This calculated approach slab change in length was then also used in Section 6.3.3 as part of the field abutment displacement calculation.

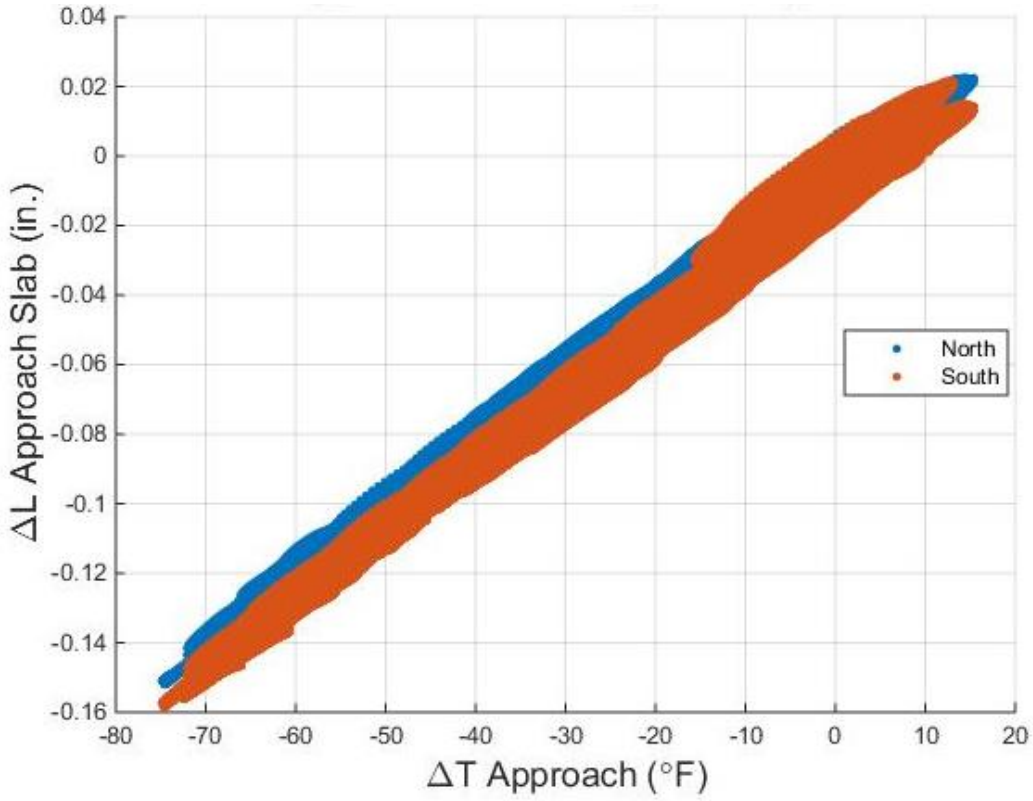

Figure 26. Approach slab change in length (Kishwaukee).

To gain an overall sense of the *stress* imparted on the approach slab, a second correction was applied to the original strain measurement in order to obtain the load-related strain. This calculation needs to account for the fact that strains due to unrestrained thermal expansion and contraction would not impart a stress on the slab. Therefore, the load strain was calculated by correcting the original strain measurement for both the thermal effects on the gage itself and the strain related to free thermal expansion and contraction of the slab, as given by:

$$\Delta\varepsilon_{load} = \Delta\varepsilon_{measured} + \Delta T_{Approach\ Slab} \times \left(\alpha_{gage\ steel} - \alpha_{concrete}\right) \qquad (2)$$

where $\alpha_{concrete}$ is the coefficient of thermal expansion of the approach slab (assumed to be 5.5 microstrain/°F).

The resulting load-related strain calculated from equation 2 above represents the strain in the approach slab due to external forces or restraint, which would lead to stress in the slab. Continuing with the assumption that that the approach slab remains in the elastic regime, the load strain was converted to load stress using Young's modulus of the slab. To analyze the results further, a representative hot and cold day during the first year of data collection were chosen, which represent

changes in temperature of +10°F and -70°F, respectively. Analyzing load stress results from each individual gage demonstrates that the approach slab load stress is not uniform throughout the approach slab, as seen in Figure 27. The highest magnitude stress was observed at mid-width of the approach slab closer to the expansion joint. These differences in stress could be in part due to differences in soil friction between the soil and underside of the approach slab, or from differences in restraint levels on different sides of the approach slab.

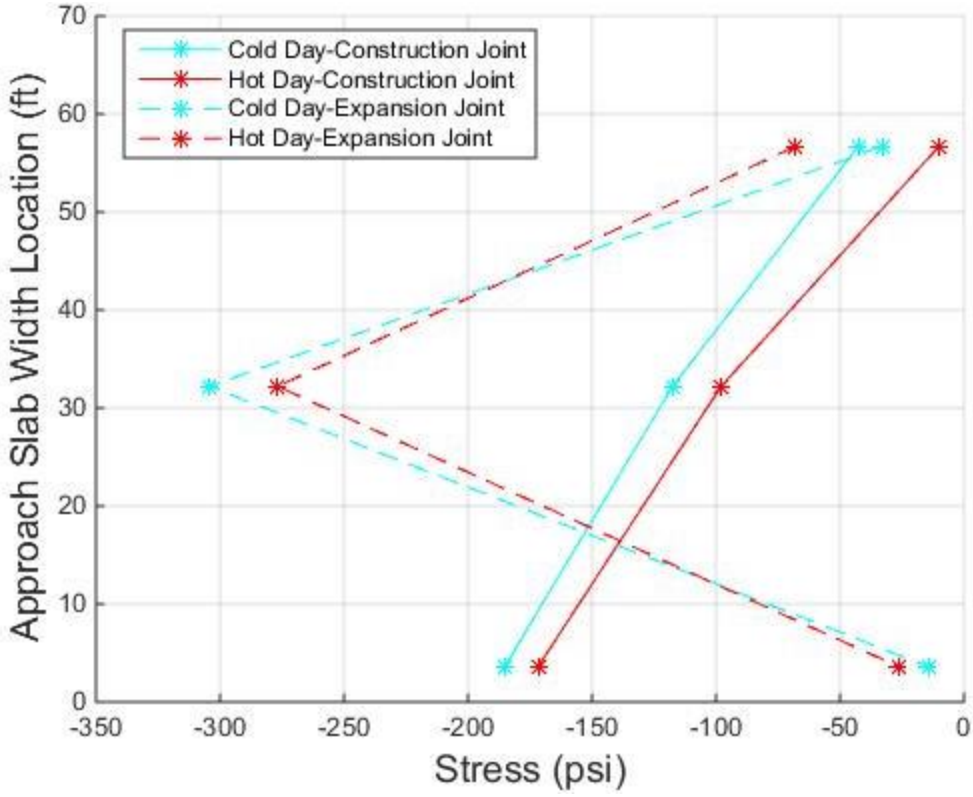

Figure 27. Kishwaukee approach slab stress near construction and expansion joint on hot- and cold-day.

To gain a better overall understanding of the approach slab behavior, the average of all the individual approach slab load stresses was taken. Results show stress magnitudes within expected ranges, and the calculated stress in the approach slab over time displays clear seasonal trends. However, there is a shift (decrease in slope) in the magnitude of stress after every year of data collection, as seen in Figure 28. The initial shift (shown in blue) occurred after the first four months of data collection and could likely be attributed to construction activity. Thereafter, the data follows a more consistent linear trend with change in temperature, however the slope decreases after each summer. As the slope decreases, the approach slab stress becomes more constant and seems to indicate a decrease in restraint, thus allowing the approach slab to displace more freely.

This could in part be attributed to soil settlement beneath the approach slab, which would reduce the friction on the bottom surface of the approach slab after each annual cycle. This shift is also similar (and could be related) to the shift seen in the approach – transition slab displacements in Figure 23, where the bridge overcomes some resistance and the expansion joint closes further than in the previous year.

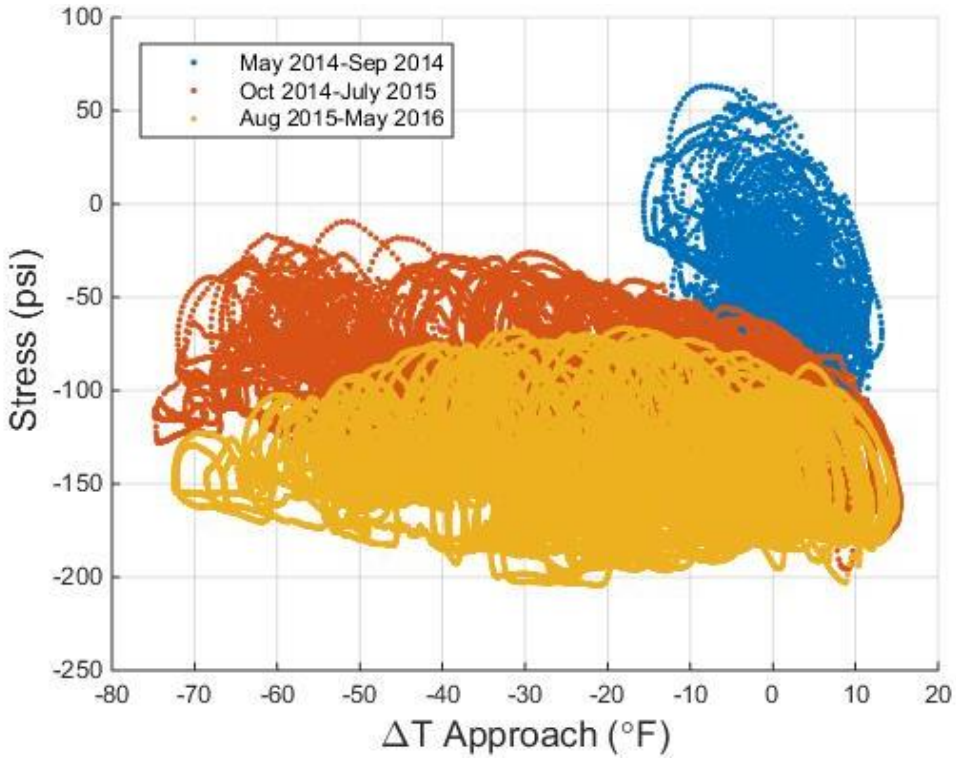

Figure 28. Average approach slab stress vs. change in temperature (Kishwaukee).

6.3.3 Abutment Displacements

As stated earlier, a major point of interest for IABs is the longitudinal bridge displacement at the deck level, which can be taken from the abutment movement. Since there was no direct measurement of abutment displacement in the field, the displacements were calculated utilizing the crackmeter and approach slab strain gage measurements, along with other certain necessary assumptions. Due to the location in which the crackmeters were installed, the measurements are of relative displacement, making it difficult to distinguish which component is actually moving in an absolute sense (e.g., the abutment moving versus the approach slab moving). In order to calculate the abutment displacement, a fixed reference point had to be determined. In this case, the transition slab was assumed to be fixed and utilized as the fixed reference point. The field

displacement of the north and south sides of the abutment were then calculated as the sum of the approach slab change in length calculated from the strain gages (Figure 26) and approach slab – transition slab and approach slab – abutment crackmeter displacements. Due to the previously mentioned shift in approach slab – transition slab measurements, the resulting field abutment displacements also show a shift after the first year of data collection. These calculated abutment displacements are compared to the abutment displacement results from the FE model in Figure 29 and Figure 30. Since the east abutment and approach slab were instrumented, a negative displacement indicates that movement is towards the bridge, signifying bridge contraction.

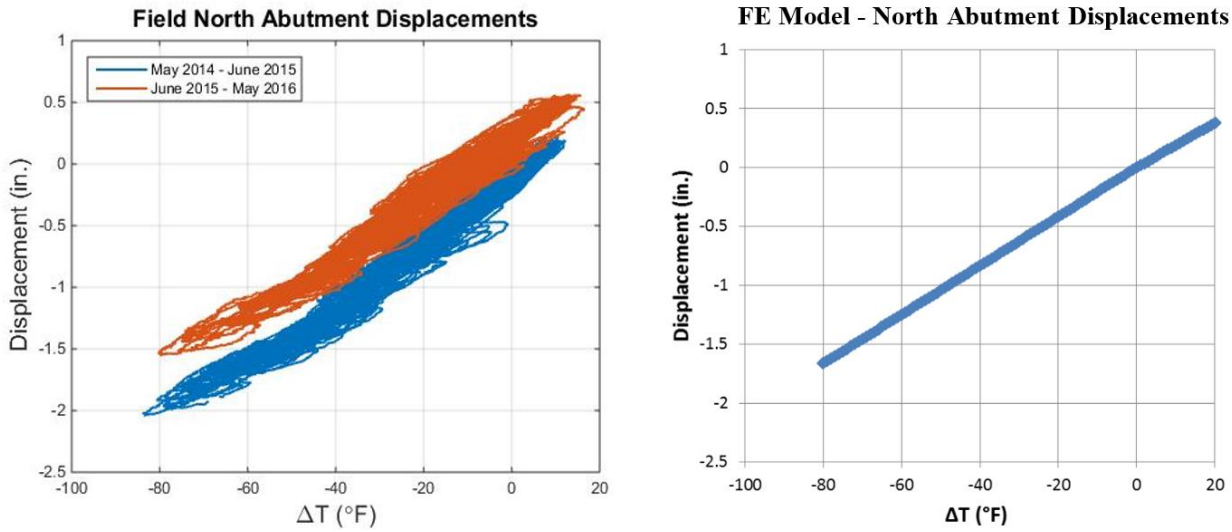

Figure 29. Comparison of Kishwaukee east-abutment north side longitudinal displacement.

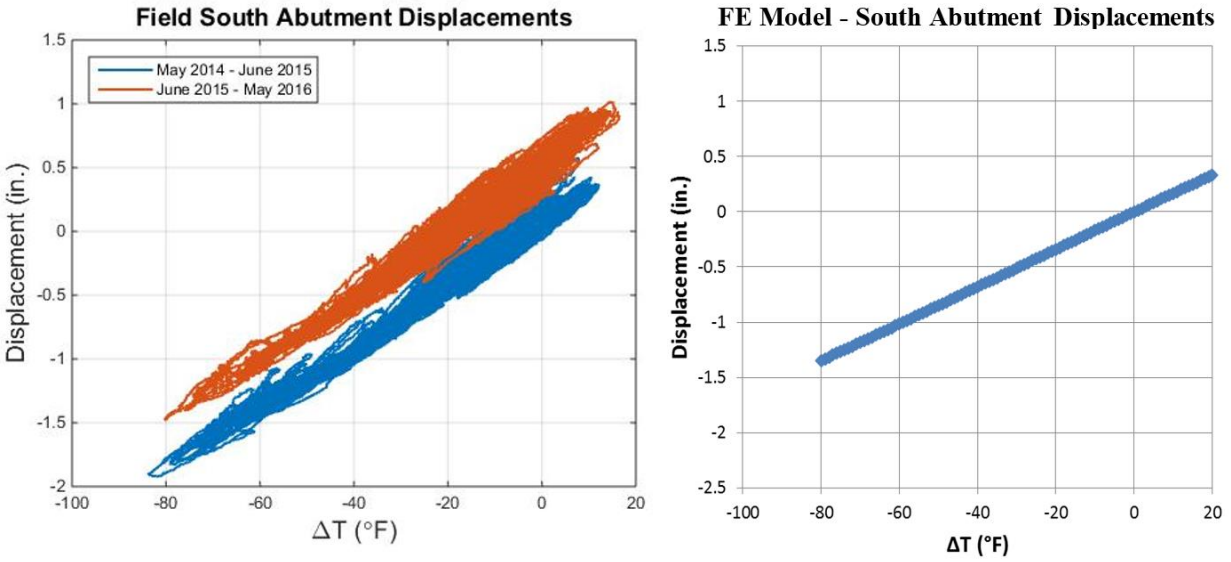

Figure 30. Comparison of Kishwaukee east abutment south side longitudinal displacement.

Despite the shift in displacement after the first year of data collection, the trends seen in the calculated field abutment displacements align well with the abutment displacements reported from the FE model, especially for the field data from the second year of monitoring (June 2015 - May 2016). Field results from the first year of data collection are slightly more extreme in contraction than what is seen in the model. Even with these slight differences, both the field and model data demonstrate larger longitudinal movement near the north side of the abutment, near the bridge's acute corner. Further analysis of the FE model data demonstrates that Kishwaukee (and UPRR) exhibit greater longitudinal movement of the acute corner as compared to the obtuse corner. Model results from both bridges also depict both longitudinal and transverse bridge movement occurring, as shown in Figure 31. This bi-directional movement is a result of the abutment skew of the bridges – Kishwaukee with 30° skew and UPRR with 42.5° skew. Both of these observations from the field and model data support findings from the parametric study, which concluded that bridges with mild to high skew (approximately 35° or greater) exhibit unsymmetrical displacements of the acute and obtuse corners, causing overall movement more towards the acute corners (LaFave et al. 2016).

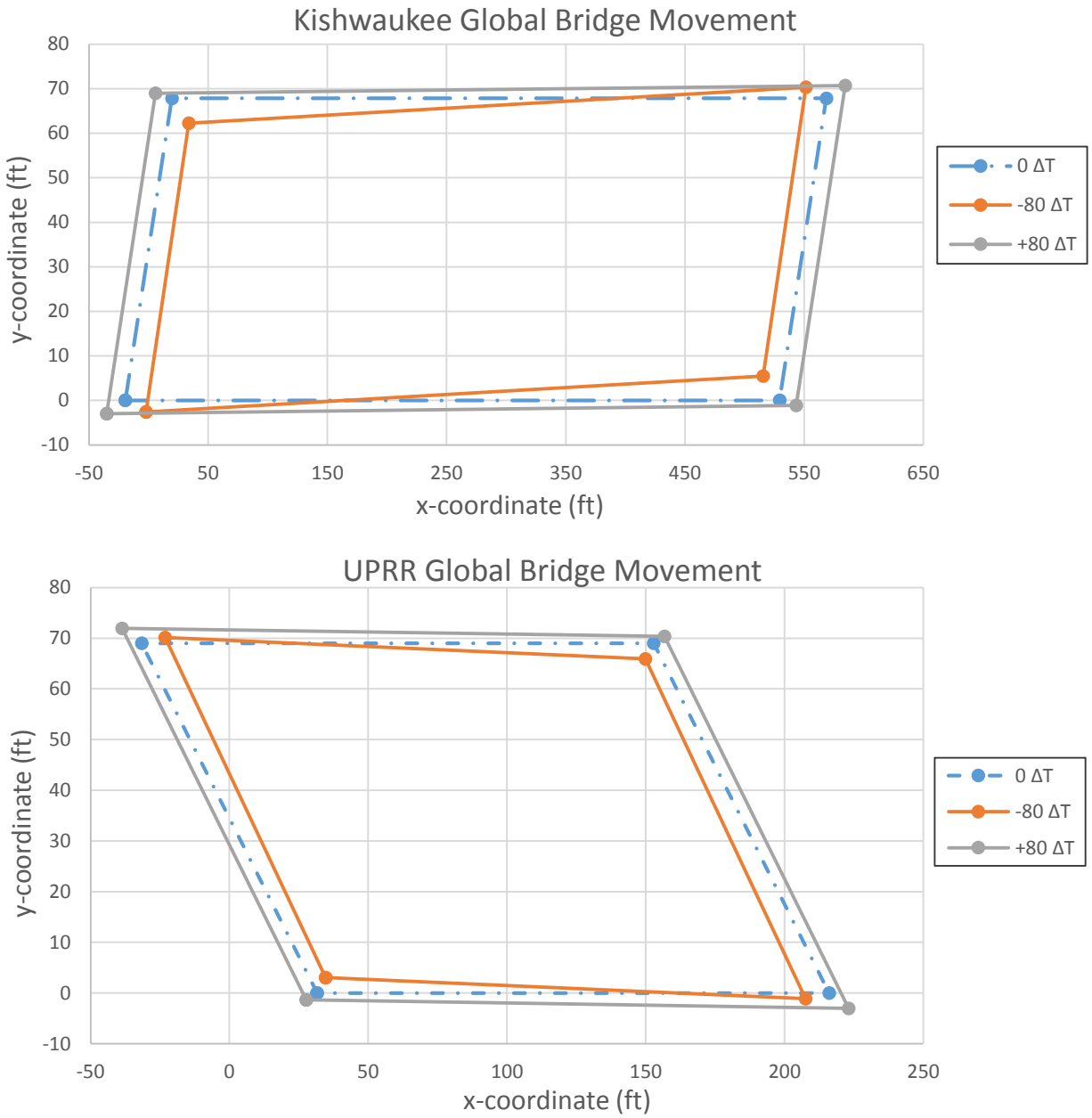

Figure 31. Kishwaukee (top) and UPRR (bottom) FE model global bridge movements due to change in temperature (125x scale).

6.4 ROTATION MEASUREMENTS

One of the main objectives of the field instrumentation was to evaluate the level of fixity at several interfaces of the abutment, in order to validate previous modeling assumptions. To do so, both individual tiltmeter measurements and calculated relative rotations were analyzed. As previously mentioned, tiltmeters were installed at certain girder ends and above and below the abutment cold joint. The labeling convention is shown in Figure 32 for reference. All of the individual rotation

measurements (and thus also the calculated relative rotations) from both bridges demonstrated a linear trend with change in temperature. However, the rotation results appeared in bands, with the majority of the data concentrated in one middle band, as seen in Figure 33. This central band is present throughout the entire data collection period, as seen in Figure 34, indicating the other bands are not due to a sudden shift to a new position. Since the majority of the data is contained in the central band, it is likely that the other bands are due to different live load scenarios along with some limited abutment cracking, allowing different levels of rotation at times.

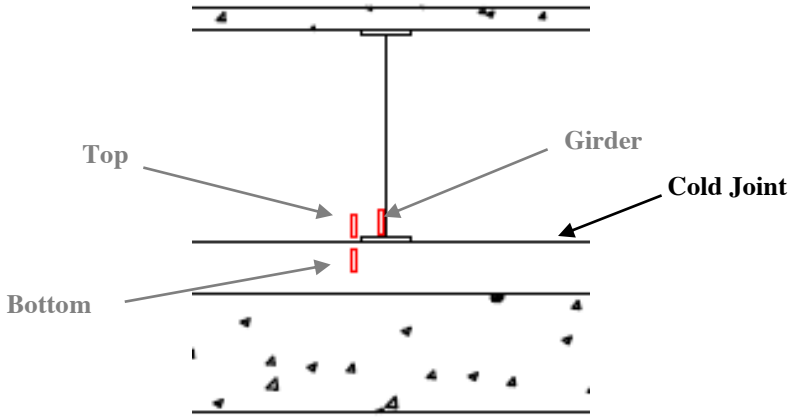

Figure 32. Tiltmeter labeling convention at an abutment.

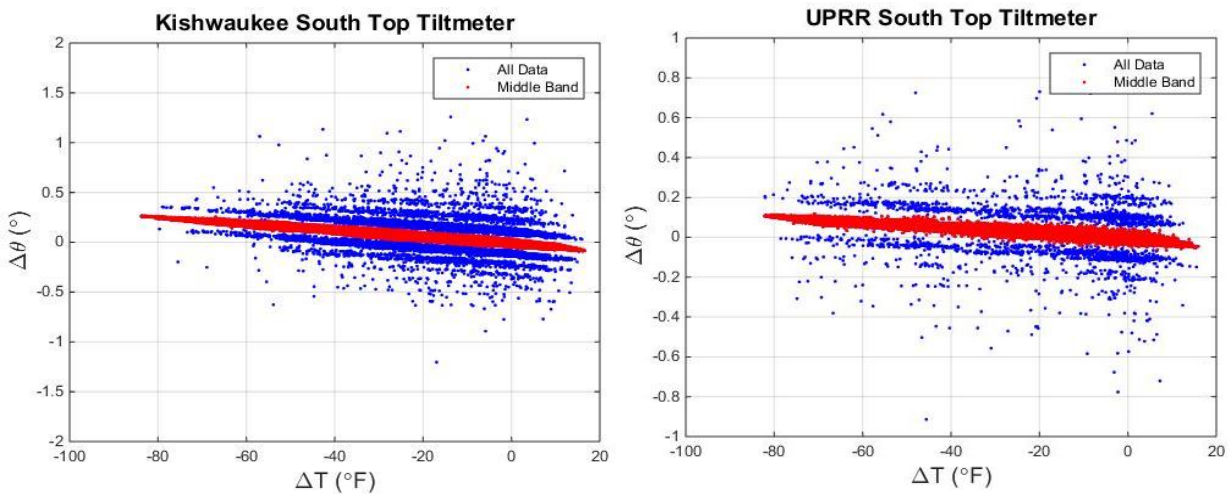

Middle band = 93% of total data

Middle band = 94% of total data

Figure 33. Kishwaukee and UPRR south top tiltmeter rotation vs. change in temperature.

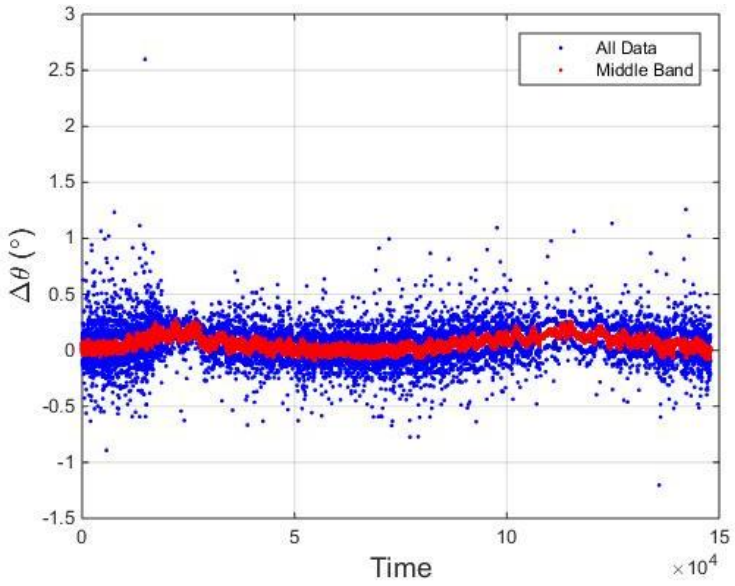

Figure 34. Kishwaukee south top tiltmeter vs. time.

The main objective of the tiltmeter measurements was to determine the field rigidity of the abutment cold-joint and girder-abutment connections. To analyze the cold-joint rigidity, the differential rotation between the upper-diaphragm (top tiltmeter) and lower-footing (bottom tiltmeter) regions of the abutment was calculated. Analyzing the central band of results, the cold-joint differential rotation at both the north and south sides of the abutment of both bridges is essentially zero at all temperatures, as seen in Figure 35. This validates the fully continuous (and uncracked), moment-resisting connection assumption that was used in the FE models of the instrumented bridges and as part of the previous parametric study models.

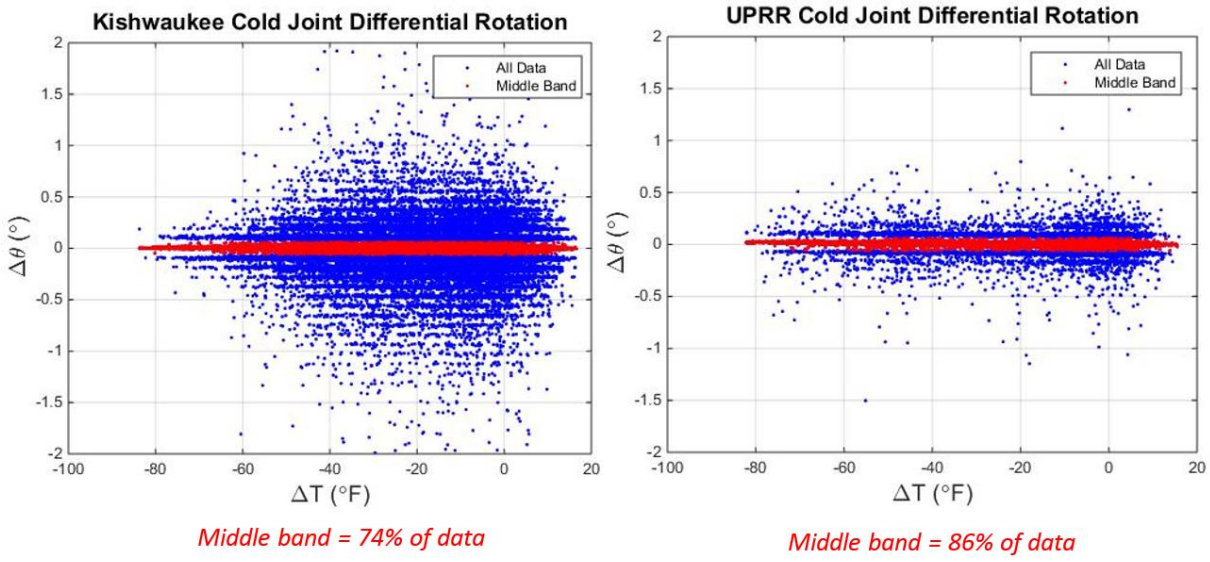

Figure 35. Cold-joint differential rotations for the south side of the Kishwaukee and UPRR abutments.

The rigidity of the girder-abutment connection was analyzed by calculating the differential rotation between the girder end and corresponding abutment top tiltmeter. In both the instrumented bridge models and parametric study models, this connection was assumed to be rigid. However, unlike at the cold joint, field results demonstrate that there is some slight differential rotation between the abutment and girders at both bridges, as seen in Figure 36. At Kishwuakee, this differential rotation is greater at the north and south ends of the abutment, as compared to that at the middle. Upon further analysis, it was determined that the three top tiltmeters (north, middle, and south) displayed roughly the same amount of rotation. However, the north and south girder tiltmeters exhibited almost no rotation, causing a large differential rotation. The middle girder tiltmeter exhibited a rotation of almost the same magnitude as the middle top tiltmeter, causing the lower magnitude differential rotation at this location. At UPRR no such comparison can be made, as there was no girder tiltmeter at the center of the abutment. However, the north and south girder-abutment differential rotation results were very similar to each other.

Focusing on the girder-abutment differential rotation central band of data, the maximum differential rotations measured 0.33° and 0.29° at Kishwaukee, and 0.1° and 0.08° at UPRR, for the north and south sides, respectively. The central band absolute maximum girder–abutment differential rotation occurred at the north side (near the acute corner) of both bridges, as presented in Figure 36. In order to assess the level of rigidity of these connections, the field observed rotations were compared to a simple hand-calculation. Since UPRR is a single-span bridge, it was possible to conduct a hand-calculation to determine the expected end rotation for a simply-supported superstructure (pinned-pinned) case. For this pinned scenario, the differential rotation at the yield moment was approximately 1.06° for a fully composite section and 1.92° for a noncomposite section. The 0.1° differential rotation observed at UPRR is much smaller than the pinned-pinned scenario, and thus the connection appears to be much closer to a continuous/rigid connection than a pinned one. Similarly, extrapolating this data to the field results at Kishwaukee, the girder-abutment connection seems to behave more as a continuous/rigid than pinned connection. Therefore, the field results validate the assumption of a rigid girder-abutment connection for purposes of the instrumented bridge models and parametric study models.

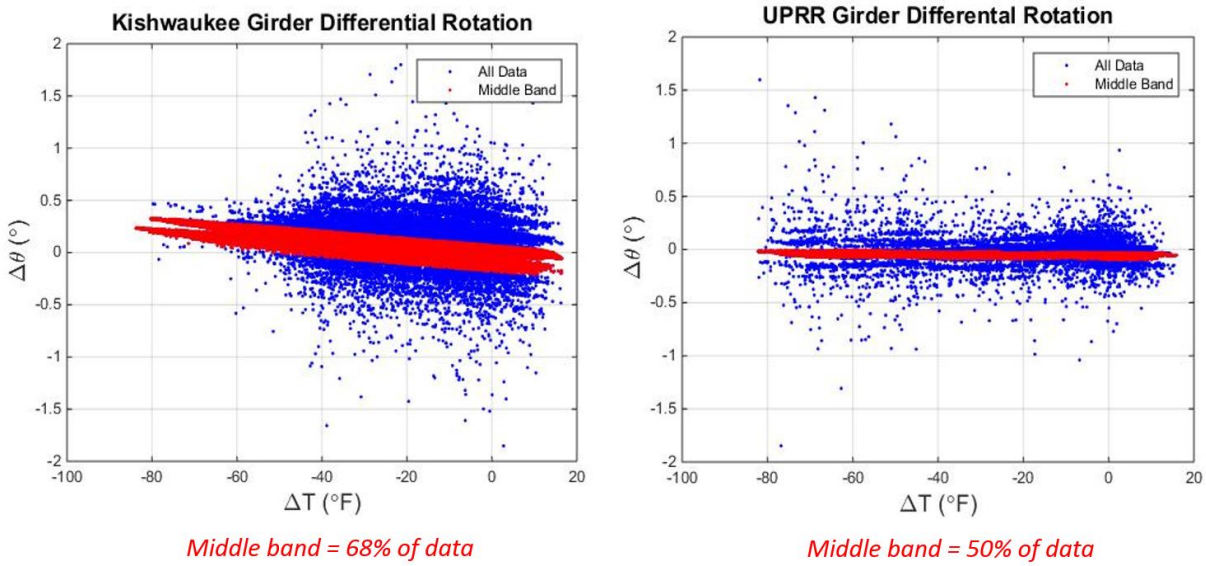

Figure 36. Differential rotation between the abutment and girders at the north side of the Kishwaukee and UPRR abutments.

In order to better understand the effects of assuming a rigid girder-abutment connection, a limited sensitivity study was conducted to investigate the modeling effects of using rigid versus only partially-restrained girder–abutment connections. The Kishwaukee Bridge model was used as a basis for this study since it displayed the larger magnitude of measured field girder–abutment differential rotation. The original Kishwaukee model with rigid girder-abutment connections was compared to two new Kishwaukee Bridge models, one with partially rigid girder–abutment connections and one with nearly pinned girder–abutment connections. No other aspects of the model were changed. As expected, the two new models exhibited an increase in girder–abutment differential rotation, as compared to the original Kishwaukee model. Analyzing the pile and girder results indicated that the different connections also have an effect on the superstructure and substructure demands. The FE model bottom flange girder stresses at the abutment (location of highest girder stress) decreased in magnitude as the girder–abutment connection rigidity decreased, as seen in Figure 37. Bottom flange girder stresses along the length of the middle girder decreased overall, with only a small increase in magnitude seen at the exterior pier location. Overall, the model with pinned-pinned girder–abutment connections displayed the lowest magnitude girder stresses. Similarly, the piles also exhibited a decrease in peak pile strains as girder–abutment connection rigidity decreased. However, the pile strains did demonstrate increased combined flexure behavior, likely due to the increased flexibility allowing for more bi-directional abutment movement.

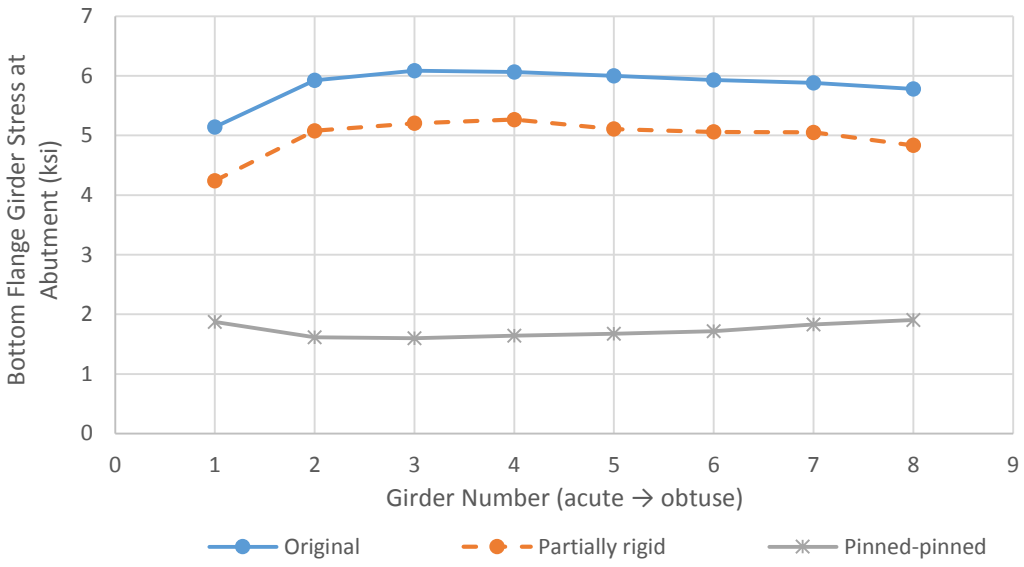

Figure 37. Comparison of Kishwaukee girder stresses at the abutment for -80° pure negative thermal load case.

Results from this sensitivity study seem to indicate that implementing a rigid girder–abutment connection in the FE model is slightly conservative in cases where there is indeed some limited flexibility at the girder–abutment connection in the field. The actual level of fixity of the instrumented bridges cannot be determined exactly and may even be variable over time. Therefore, the girder–abutment connections of the final versions of the instrumented bridge models were not modified; they simply utilized a rigid-connection assumption, as this provides slightly conservative and yet reliable results. Furthermore, the sensitivity study indicates that a fully continuous, moment-resisting connection assumption is appropriate for the purposes of this project. The results provide slightly conservative results, further validating findings from the previous parametric study phase.

6.5 PILE DEMANDS

The limited instrumentation installed on the bridge piles helped provide an overall understanding of the IAB substructure behavior to complement the superstructure findings. The pile gages were installed in sets of four (4), as seen in Figure 7, in order to provide data about both bending axes of the piles. Strain data from each individual gage displays a clear trend over the entire period of data collection due to change in temperature, as seen for the Kishwaukee acute pile gages in Figure

38. Each strain gage also experiences cycles of differential compression/tension on a daily basis due to daily variations in temperature.

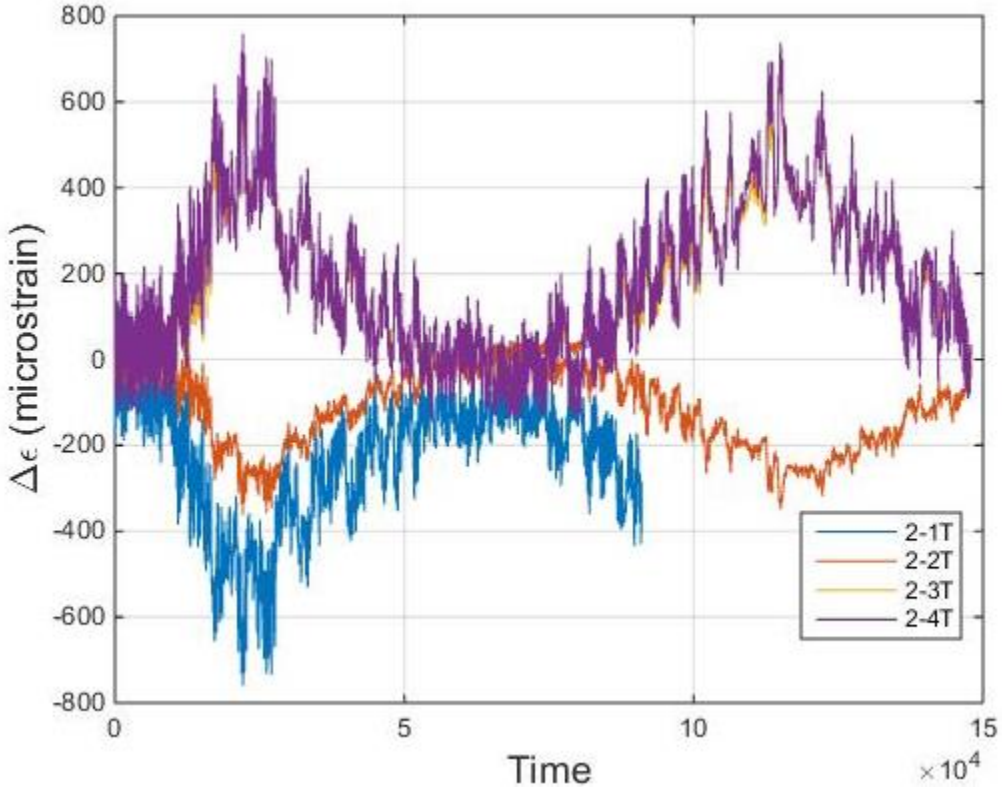

Figure 38. Kishwaukee acute pile strains throughout the entire data collection period.

Results from each set of four (4) pile gages at both bridges were plotted against change in superstructure temperature, and all exhibited a clear linear trend. Pile strains from the FE models at the corresponding gage locations were also analyzed and plotted versus change in temperature. Figure 39 through Figure 41 compare the field results of each pile at Kishwaukee to the corresponding FE model results and indicate that the model slightly overestimates the field pile strains. The UPRR model also slightly overestimates the observed field pile strains, as seen in Figure 42 through Figure 44. Site conditions at UPRR, including the MSE wall and sandy soil, may not have been fully captured by the model, which likely accounts for a significant portion of the differences between the model and field data. Additionally, slight differences between both models and the corresponding field data were expected, as the bridge models do not include vertical friction acting along the piles, and the nature of loading differs somewhat from that in the field. In the models, monotonic thermal loading was implemented, however in the field the temperature went through daily and seasonal cycles which are not fully captured with the

monotonic loading. However, both the field and model data exhibit the same linear trends with change in temperature and peak pile strains at the acute pile. Therefore, the overall similarity between the field and model data support that the use of monotonic loading is sufficient for the purposes of this project.

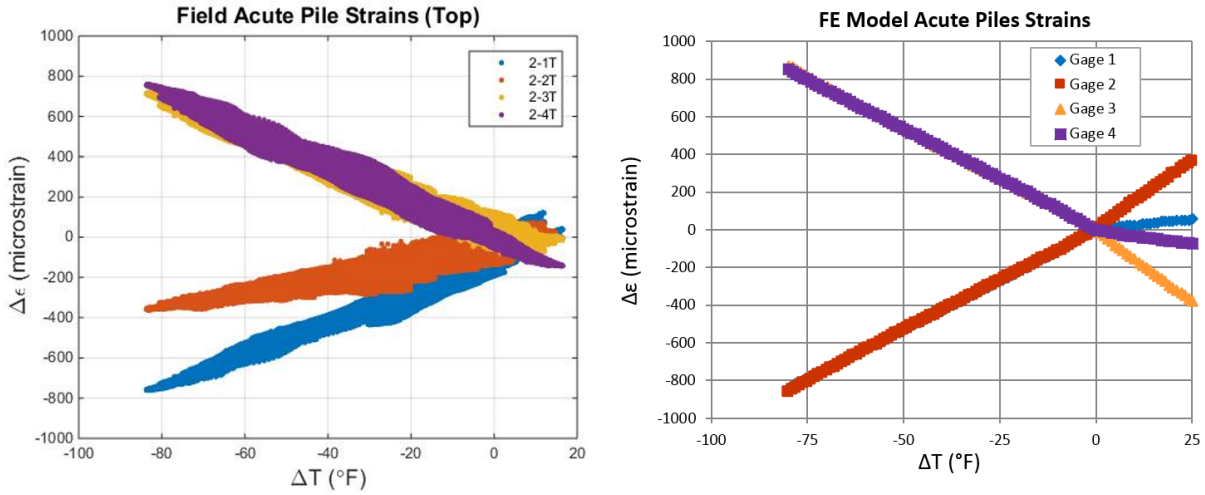

Figure 39. Kishwaukee acute (north) pile head strains.

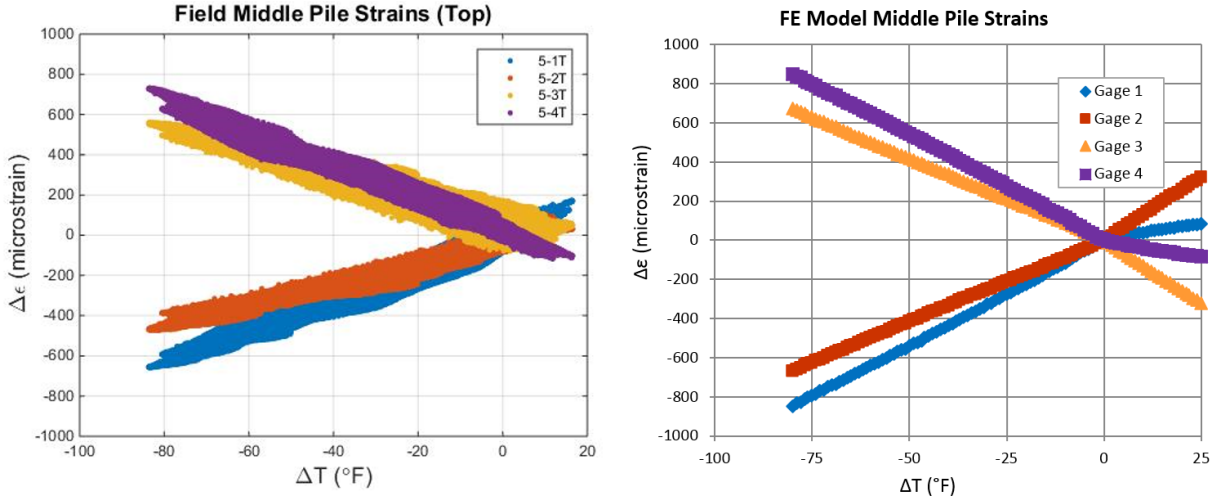

Figure 40. Kishwaukee middle pile head strains.

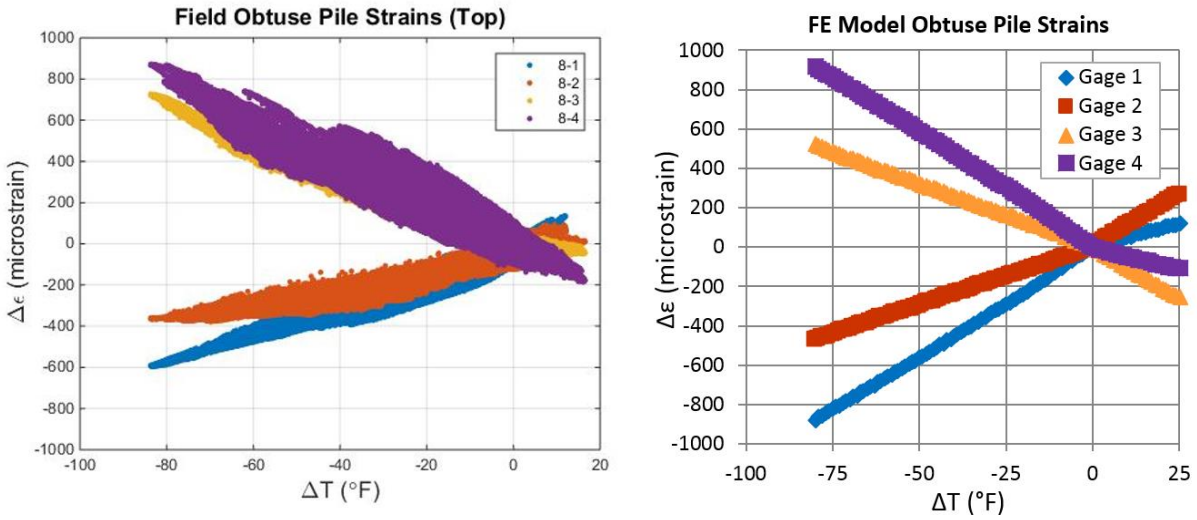

Figure 41. Kishwaukee obtuse (south) pile head strains.

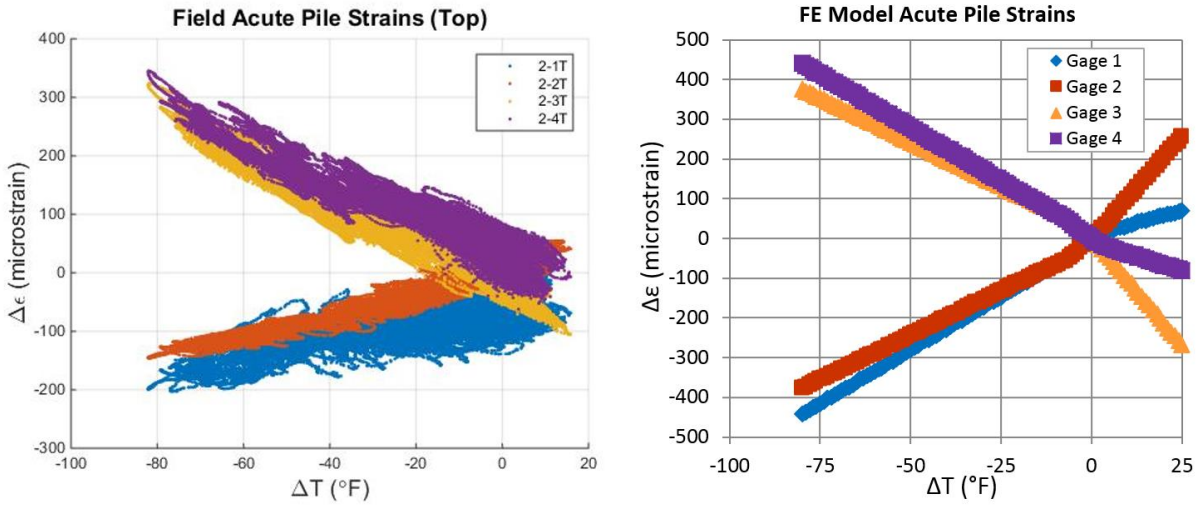

Figure 42. UPRR acute (north) pile head strains.

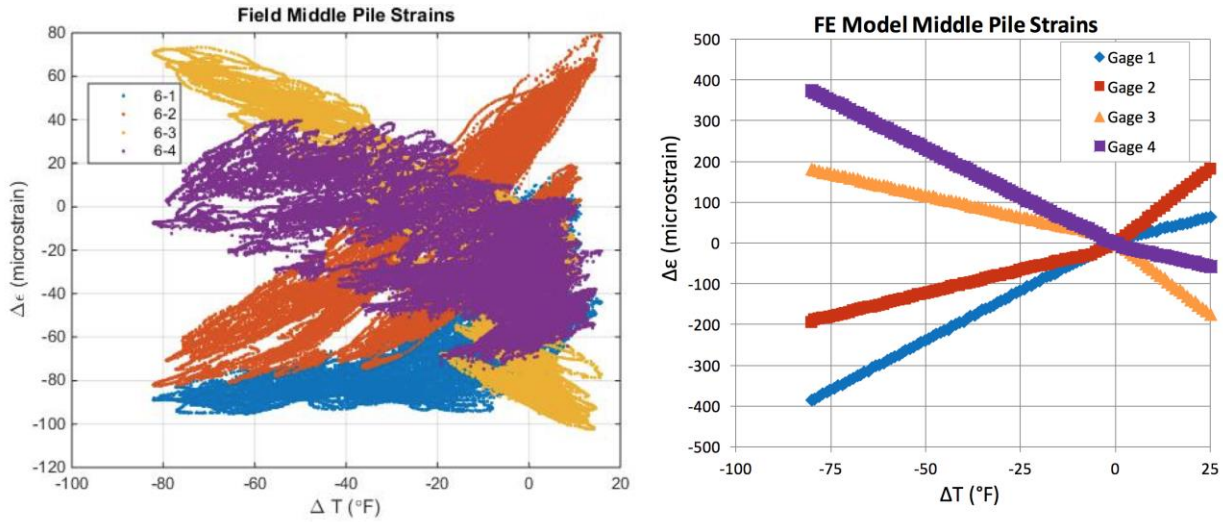

Figure 43. UPRR middle pile head strains.

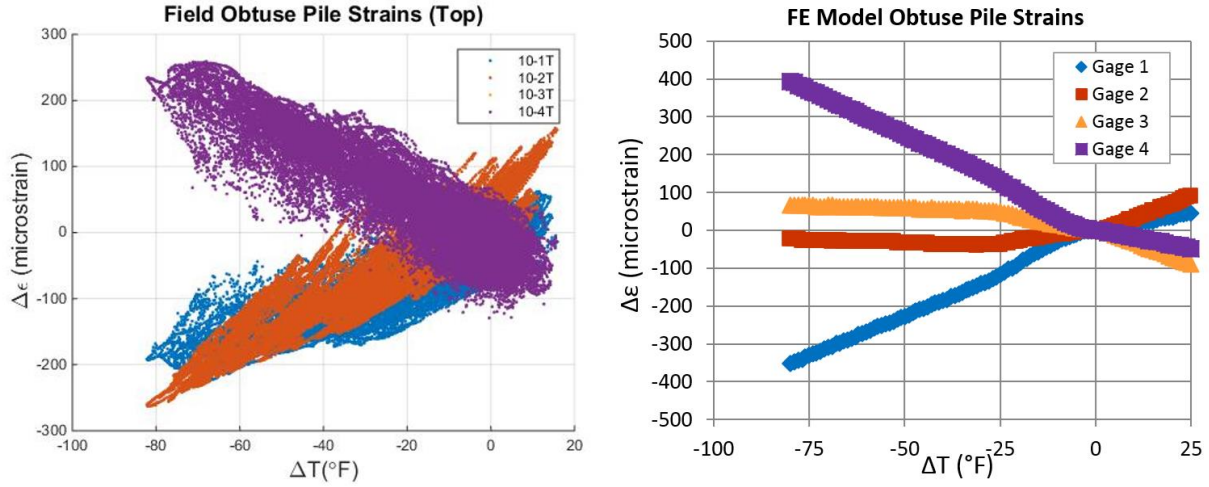

Figure 44. UPRR obtuse (south) pile head strains.

Analyzing the overall pile strain magnitudes at each bridge, both the field and model pile strains at the gage locations are lower than the yield strain of 1724 microstrain. Additionally, the field pile flange tip / extreme fiber strains were extrapolated utilizing the collected pile strains and were then compared to the corresponding flange tip data from the models. Focusing on the acute pile strains, Figure 45 and Figure 46 compare the field and model flange tip strains. The maximum model flange tip pile strains (which are greater than the field strains) for Kishwaukee and UPRR were 1705 microstrain and 852 microstrain, respectively, which are still below the yield strain. Therefore, both the slightly conservative FE models and the field data indicate that there is some

additional pile deformation capacity available, especially if some limited pile yielding is allowed, particularly at the UPRR Bridge.

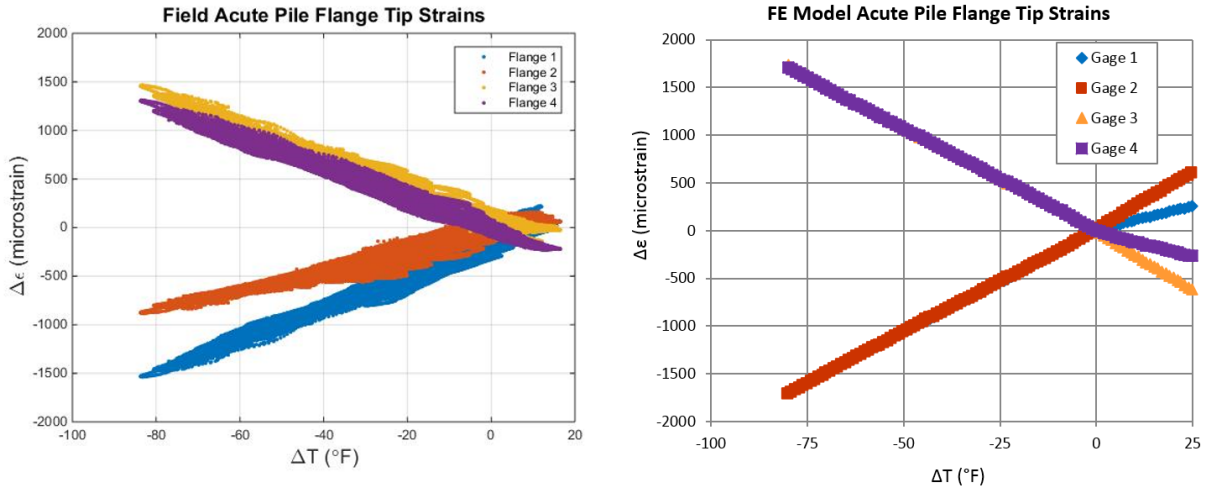

Figure 45. Kishwaukee calculated field vs. FE model pile strains at acute pile flange tips.

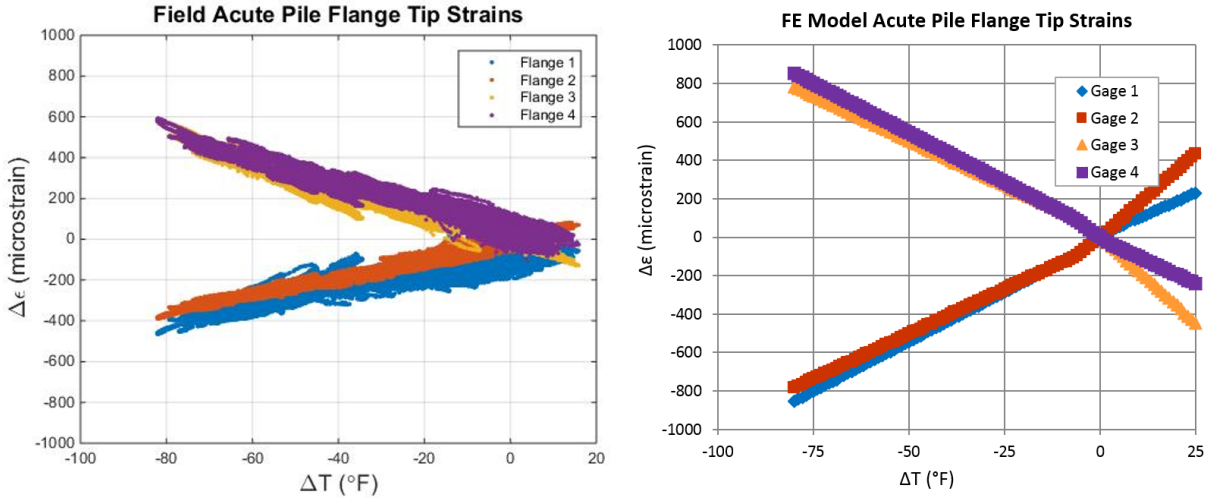

Figure 46. UPRR calculated field vs. FE model pile strains at acute pile flange tips.

The FE model data also provides further insight into what behavior accounts for the majority of the resulting pile strain. Figure 47 through Figure 49 show the model pile strains due to axial force, strong-axis bending, and weak-axis bending contributions for both the acute and obtuse piles at Kishwaukee. Similar trends are seen from the UPRR model strain components, only with overall lower strain magnitudes, as expected. This breakdown shows that the majority of the pile strains come from weak-axis bending, as expected for an IAB with weak axis oriented piles such as Kishwaukee or UPRR. Focusing on the contraction regime, the FE model axial and strong-axis

contributions increase from acute to obtuse piles in the models. The strong-axis contribution is likely what causes a separation between the gage pairs in tension and compression, and the axial force contribution is likely what causes the shift in magnitude of all the gage data from being symmetric about the zero-strain axis.

Field pile strains at Kishwaukee (Figure 39 through Figure 41) exhibit both the separation of gage pairs due to strong-axis contributions and the shift in magnitude due to axial force contributions, and both effects appear to increase from the acute to obtuse corner, as in the model. However, the Kishwaukee obtuse pile field data displayed a higher upward (tensile) shift in strain magnitude than the model, and a lower magnitude of separation between gage pairs than the model data. When comparing the UPRR piles (Figure 42 through Figure 44), the field results show only a small separation in gage pair magnitudes. The model seems to allow a greater strong-axis bending contribution than in the field, especially at the obtuse pile.

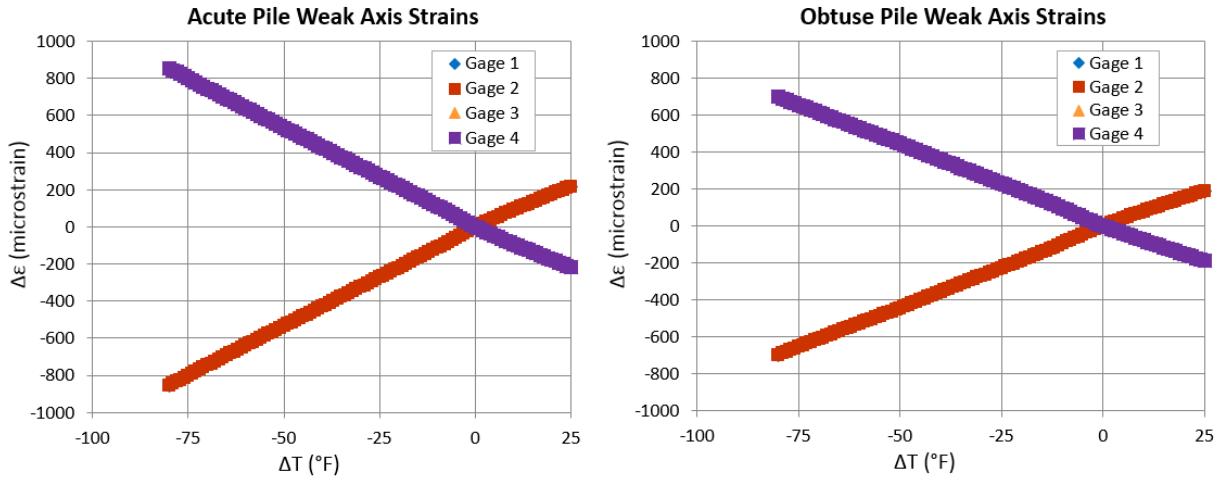

Figure 47. Kishwaukee FE model pile strains due to weak-axis bending.

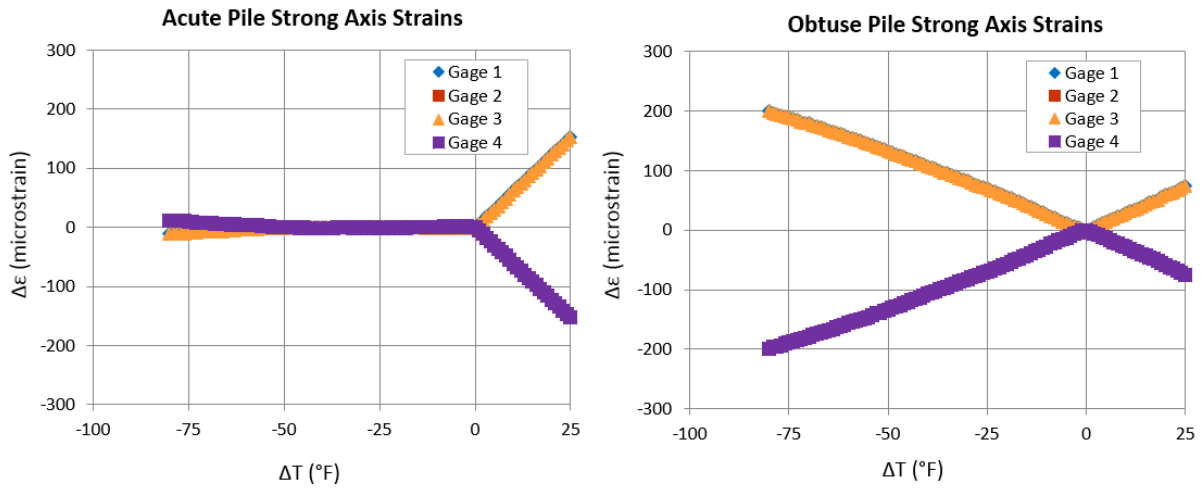

Figure 48. Kishwaukee FE model pile strains due to strong-axis bending.

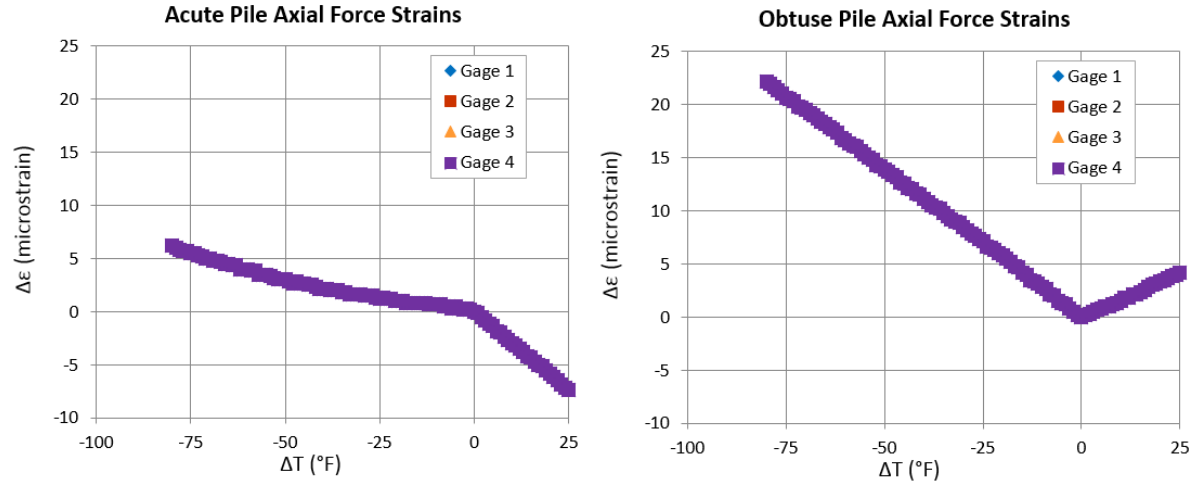

Figure 49. Kishwaukee FE model pile strains due to axial force.

Placing the strain gages on each of the pile flanges also allowed for calculation of axial force, strong-axis moment, and weak-axis moment of each instrumented pile. Figure 50 through Figure 52 show the field pile stresses at both bridges due to axial force, strong-axis moment, and weak-axis moment. The largest stress component of all of the piles comes from weak-axis moment, as seen in the model data and as expected since the piles at both bridges are placed in a weak-axis orientation. Stresses due to weak-axis moment and strong-axis moment are fairly consistent in magnitude between all the instrumented piles at each bridge. However, stresses due to axial force appear to be higher at the exterior piles. It is important to note that the middle pile at UPRR shows much lower magnitudes of total pile strain and stress components, most likely due to an error

during construction which resulted in those pile gages being approximately 8 in. higher (i.e., partially embedded up into the pile cap) than the corresponding gages on the exterior piles.

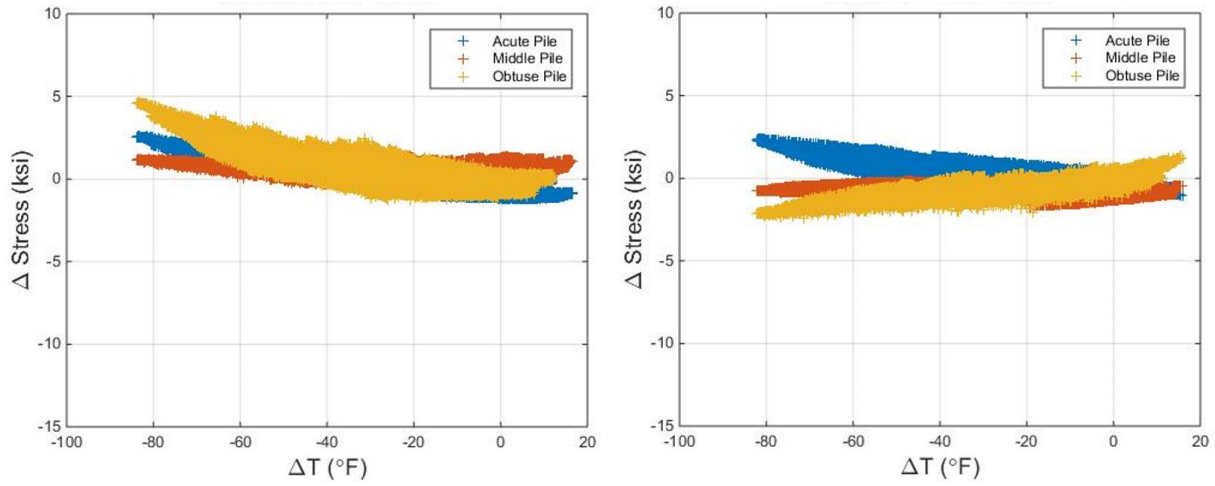

Figure 50. Pile stress due to axial force in the piles at Kishwaukee (left) and UPRR (right).

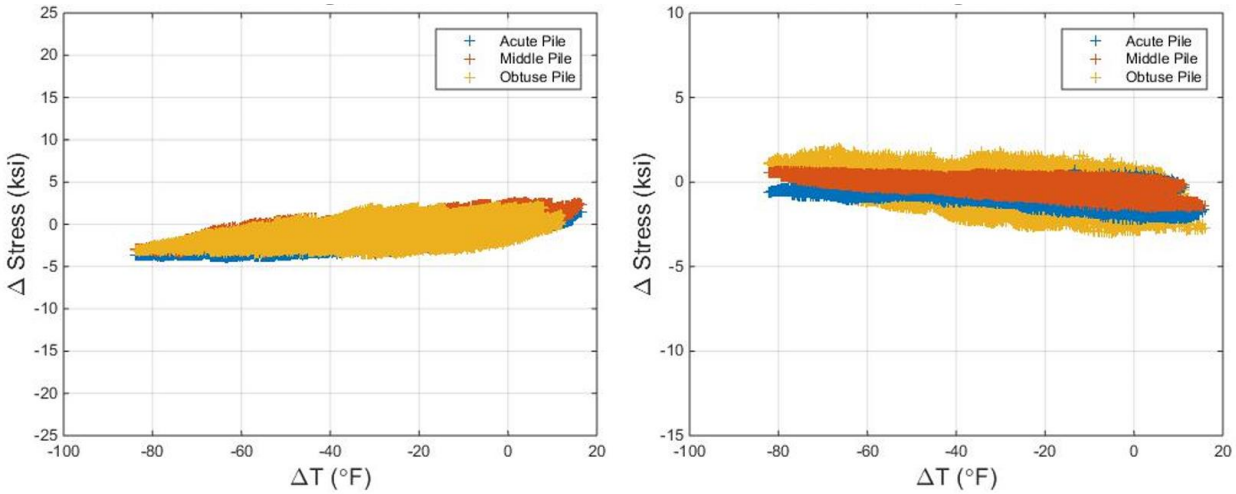

Figure 51. Pile stress due to strong-axis moment in the piles at Kishwaukee (left) and UPRR (right).

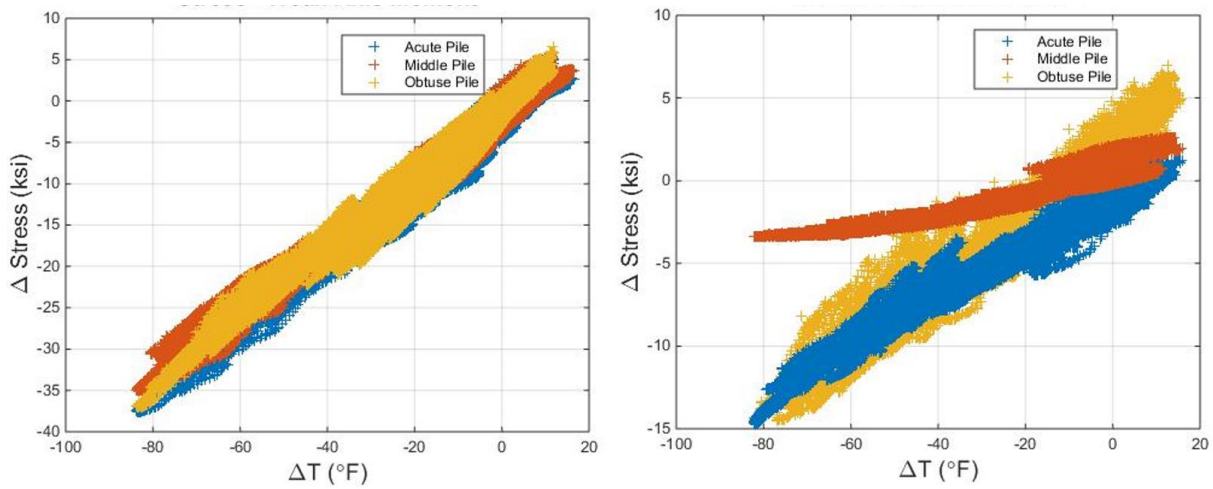

Figure 52. Pile stress due to weak-axis moment in the piles at Kishwaukee (left) and UPRR (right).

Another aspect of interest regarding pile behavior is the pile – abutment connections. For both the Kishwaukee and UPRR bridges, each pile was embedded 2 ft into the abutment, essentially creating a rigid connection. The FE models of the two bridges assume this connection to be rigid due to pile embedment. However, it is possible that there could be some flexibility present in the connection, for instance due to any cracking of the concrete surrounding the piles. This flexibility could account for a small part of the observed difference between the field and model pile strain magnitudes. No tiltmeters were placed on the piles at either bridge, so the exact level of fixity of the pile – abutment connection could not be determined experimentally. However, to investigate the general effects of modeling the pile – abutment connection as rigid versus semi-rigid, a limited analytical sensitivity study was still conducted.

The UPRR bridge model was utilized for this sensitivity study, and two new modified versions were created – one with a semi-rigid connection and one with the extreme case of a completely released (or pinned) pile – abutment connection. Both cases showed a decrease in overall pile strain magnitudes at the pile cap boundary, with the extreme pinned case having an average 90 percent decrease in peak pile strains. Increased connection flexibility reduces pile demands as the imposed pile double curvature is relieved. Therefore, if the pile – abutment connections at the two bridges did indeed experience some limited flexibility, the use of a rigid connection in the model would account for part of reason why the models slightly overestimate the field pile strains.

6.6 GIRDER DEMANDS

Data from the girder strain gages proved to be the most variable of all the gages in terms of their fluctuating and sometimes noisy data. Some of this variability can be attributed to the fact that the girder strain gages are the most exposed to the elements and have the greatest influence from live loads. In spite of this, clear trends over time and with temperature change can still be seen in the girder strain data. Low girder stresses were generally observed in the parametric study, so the girders at both bridges have been assumed to remain elastic, and thus for analysis the strain gage data has simply been converted to stress utilizing the elastic modulus. For reference, the instrumented girder cross sections are labeled in the format of <girder number> – <location number>, where the girder number is circled in black and the location number boxed in blue in Figure 53.

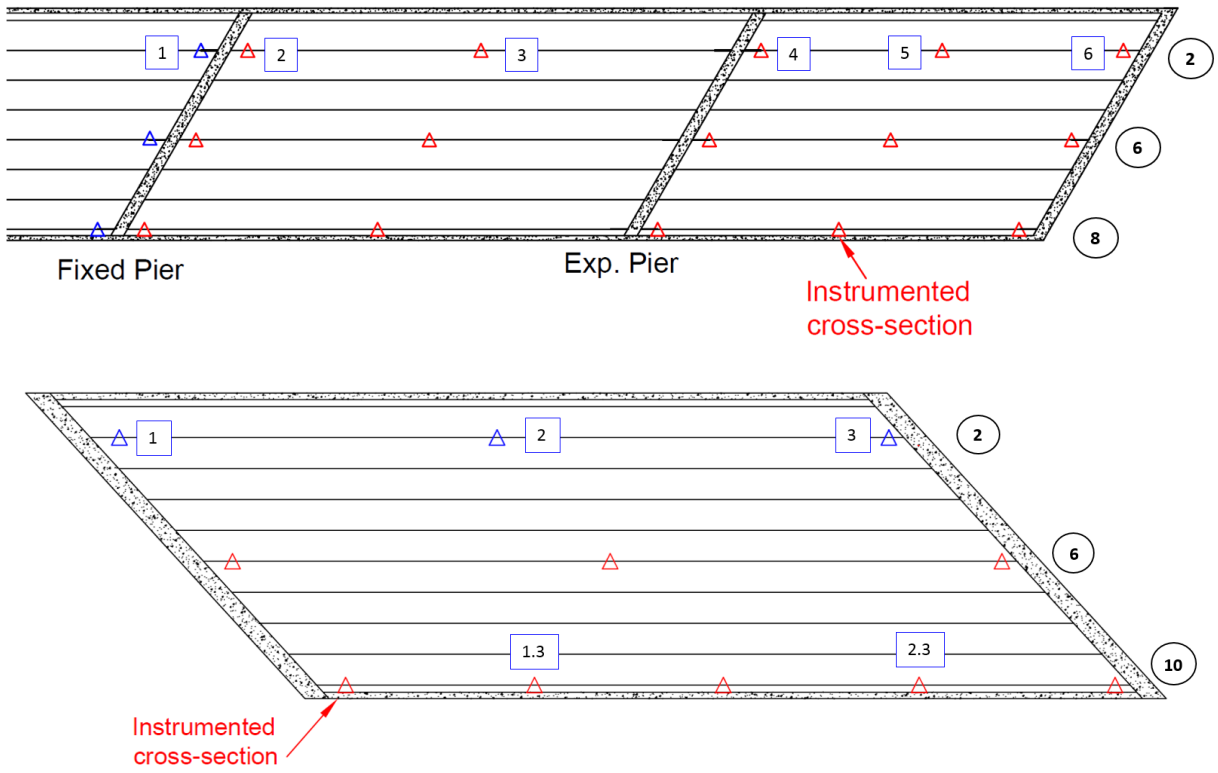

Figure 53. Girder cross-section labeling scheme for Kishwaukee (top) and UPRR (bottom).

As expected from the parametric study results, the steel girder bottom flange field data displays the highest magnitude of stresses. However, the bottom flange data is also the most variable over time. Figure 54 displays the field girder stresses from all the gages at one girder cross section for

Kishwaukee and UPRR. The field data shows that the top flange, middle, and concrete deck stresses exhibit clear trends over time due to temperature. The girder bottom flange stresses follow a similar trend for a period of time, but then tend to deviate into further tension or compression (depending on location) after approximately the first year of data collection and typically do not return back to their original state. This behavior is observed in the bottom flange data at approximately three-fourths of all the instrumented girder cross sections for both bridges; therefore, it does not appear to be an error from the gage readings, but rather some sort of systematic behavior of the girder bottom flanges.

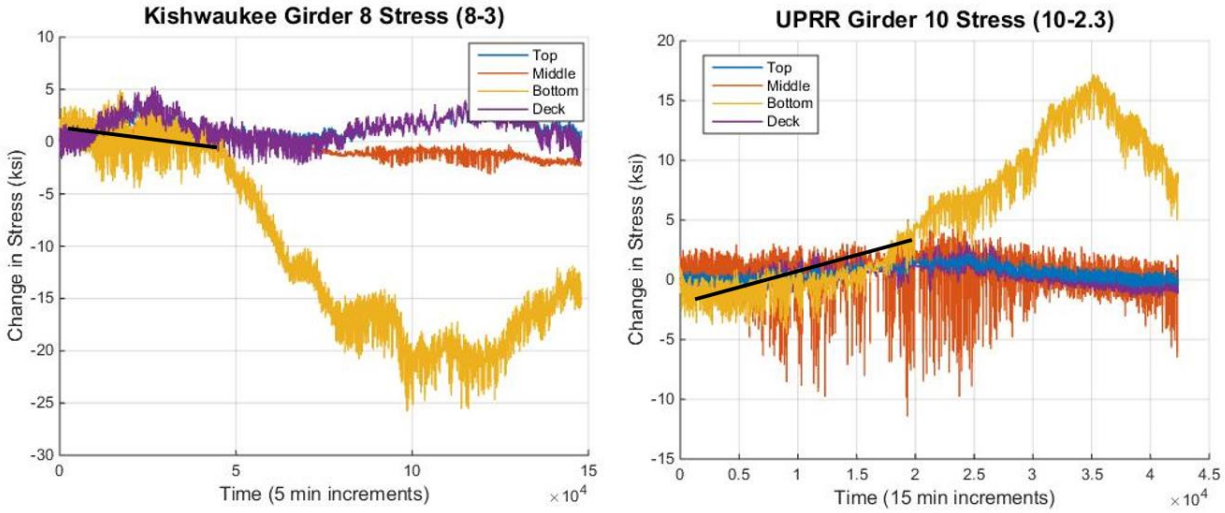

Figure 54. Girder stresses over time at Kishwaukee and UPRR.

To further analyze the field girder data, the girder top and bottom flange stresses from the instrumented bridge FE models were calculated using the strong-axis and weak-axis bending moments plus axial force at the gage locations. Both the field and model top flange data demonstrate a clear linear trend with change in temperature. Overall, the top flange field data aligned well with the FE model results, as shown in Figure 55. At a couple locations, both bridge models slightly underestimate field girder top flange stresses, but overall the top flange field data demonstrates the same overall linear trends as seen in the models.

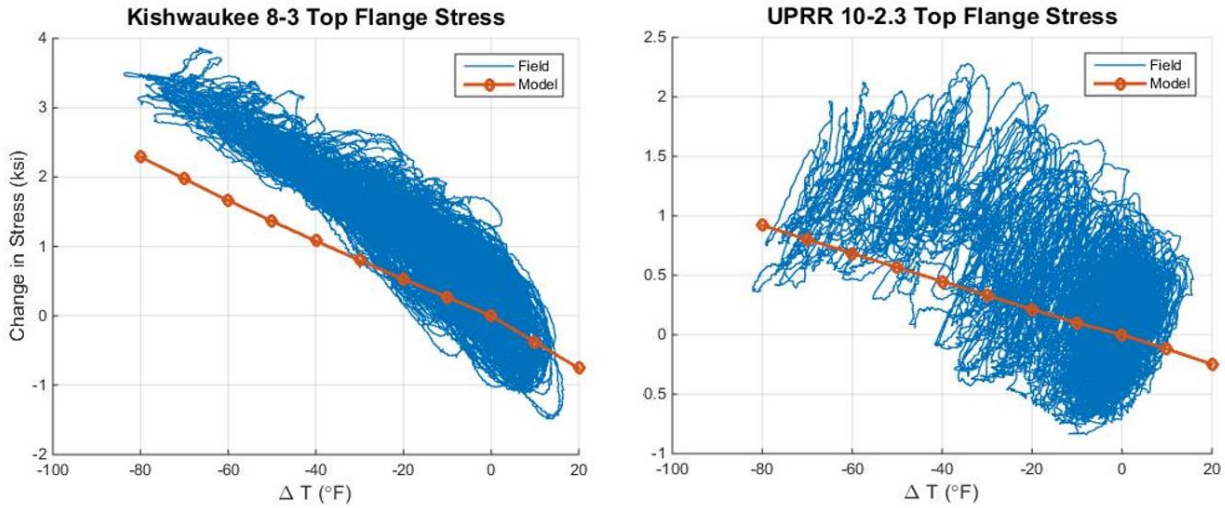

Figure 55. Top flange stress comparison of field data to FE model prediction for girder 8 interior mid-span at Kishwaukee and girder 10 east quarter-span at UPRR.

As seen in both the parametric study and from the field data, the model girder bottom flanges also displayed the highest magnitudes of stress. However, the field bottom flange stresses follow a clear linear trend with change in temperature for only part of the data. This period of time is indicated by the black line in Figure 54, which represents the first few months of data collection during which the bottom flange stresses track reasonably well with temperature. Figure 56 shows that there is fairly good correlation between the field data and FE model girder bottom flange stresses during this period of time. Further focusing on this period of time, Figure 57 shows that the model matches the field data fairly well and that both follow a clear linear relationship. After this initial period of time, though, the girder bottom flange field stresses tended to creep toward higher tension or compression values (depending on location) and deviate from the expected trends gathered from the model. This deviation seems to typically initiate after the temperature increases again during the first year and reaches a net change in temperature (ΔT) of around -40 °F, or else after once again reaching the initial temperature (0 ΔT).

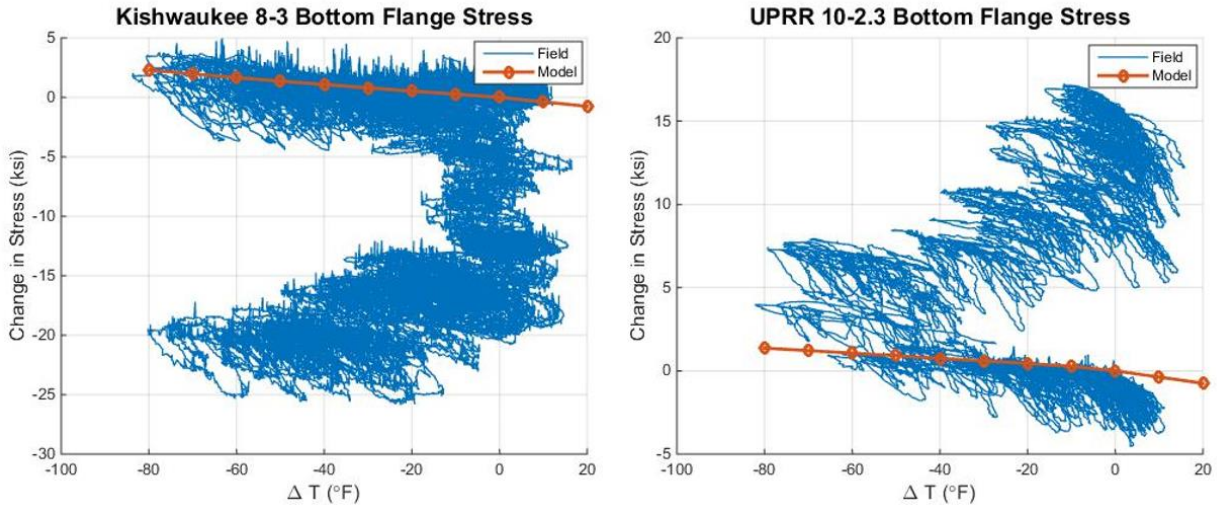

Figure 56. Bottom flange stress comparison of field data to FE model prediction for girder 8 interior mid-span at Kishwaukee and girder 10 east quarter-span at UPRR.

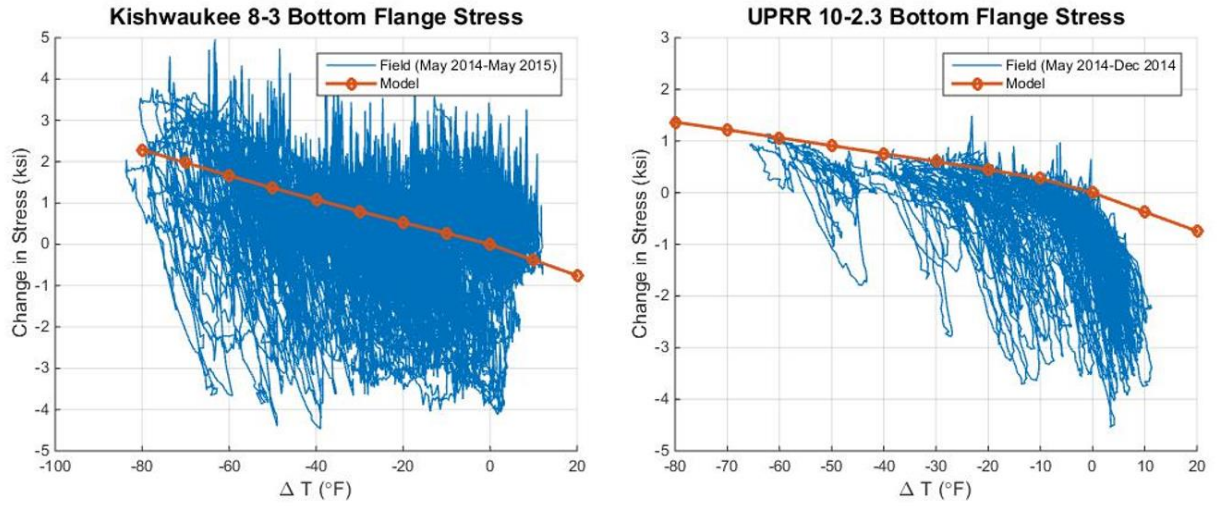

Figure 57. Bottom flange girder stress for Kishwaukee 8-3 location (May '14-May '15) and UPRR 10-2.3 location (May '14-Dec '14).

In order to further analyze what is happening along the length of each girder, specific representative "hot" and "cold" days were chosen for each year of data collection. At Kishwaukee, the representative hot days are July 22, 2014 and June 10, 2015, both of which correspond to a change in temperature of +10 °F. The representative cold days at Kishwaukee are January 7, 2015 and January 18, 2016, which correspond to a change in temperature of -80 °F. At UPRR, the representative hot days are August 24, 2014 and July 17, 2015, which correspond to a change in temperature of +10 °F. Since data collection at UPRR only lasted 16 months, there is only one

representative cold day, November 17, 2014, which corresponds to a change in temperature of -60 °F.

Figure 58 and Figure 59 compare the field and FE model top and bottom flange stresses along a girder at Kishwaukee and UPRR, respectively, on the representative hot and cold days. Focusing first on the top flange, at both bridges the top flange field stresses typically agree well with the model results during the entire period of data collection. At Kishwaukee, both the field and model top flange stresses are slightly higher near the pier and abutment. Overall, at some locations there were small deviations between the field and model results during the second year, but these typically only ranged from 1-2 ksi and were much smaller than those consistently seen from the bottom flange field results. These deviations were due to the fact that the top flange field stresses display a small increase in magnitude from the first to second year, but the general trends along the girder remain the same.

Focusing on the bottom flange, the results were much more variable. Field girder stresses from the hot and cold days during the first year of data collection (2014) were typically very similar to the predicted model results. The bottom flange stresses are typically highest in magnitude at the abutment and/or fixed pier, as expected from the parametric study trends. From the first to second year, the bottom flange field stresses typically showed a large increase in magnitude. This resulted in somewhat large differences between the field and model data, which typically varied from 5 to 15 ksi, and only in extreme cases reached up to 35 ksi. It should be noted that this increase is particularly large near the supports (including the abutments and the piers), and for UPRR also at the quarter-spans. For most mid-span locations at both bridges, the bottom flange stresses tend to stay more consistent from year to year, with only small increases in stress. Therefore, mid-span locations typically had the best correlation between girder bottom flange field and model data, while the support locations (abutment and/or piers) typically displayed much larger differences.

These large discrepancies seen in the bottom flange data could possibly be a result of out-of-plane bending of the girder's bottom flange. The cycles of bridge expansion and contraction could have caused this out-of-plane bending to result in localized yielding at some locations along the girder that are more restricted from movement, such as near the abutments and piers, which showed larger differences between the field and model data. Overall, the girder data does not provide a single

clear explanation for this unexpected bottom flange behavior, but it can be concluded that this is likely real and systematic behavior rather than just an error in gage performance.

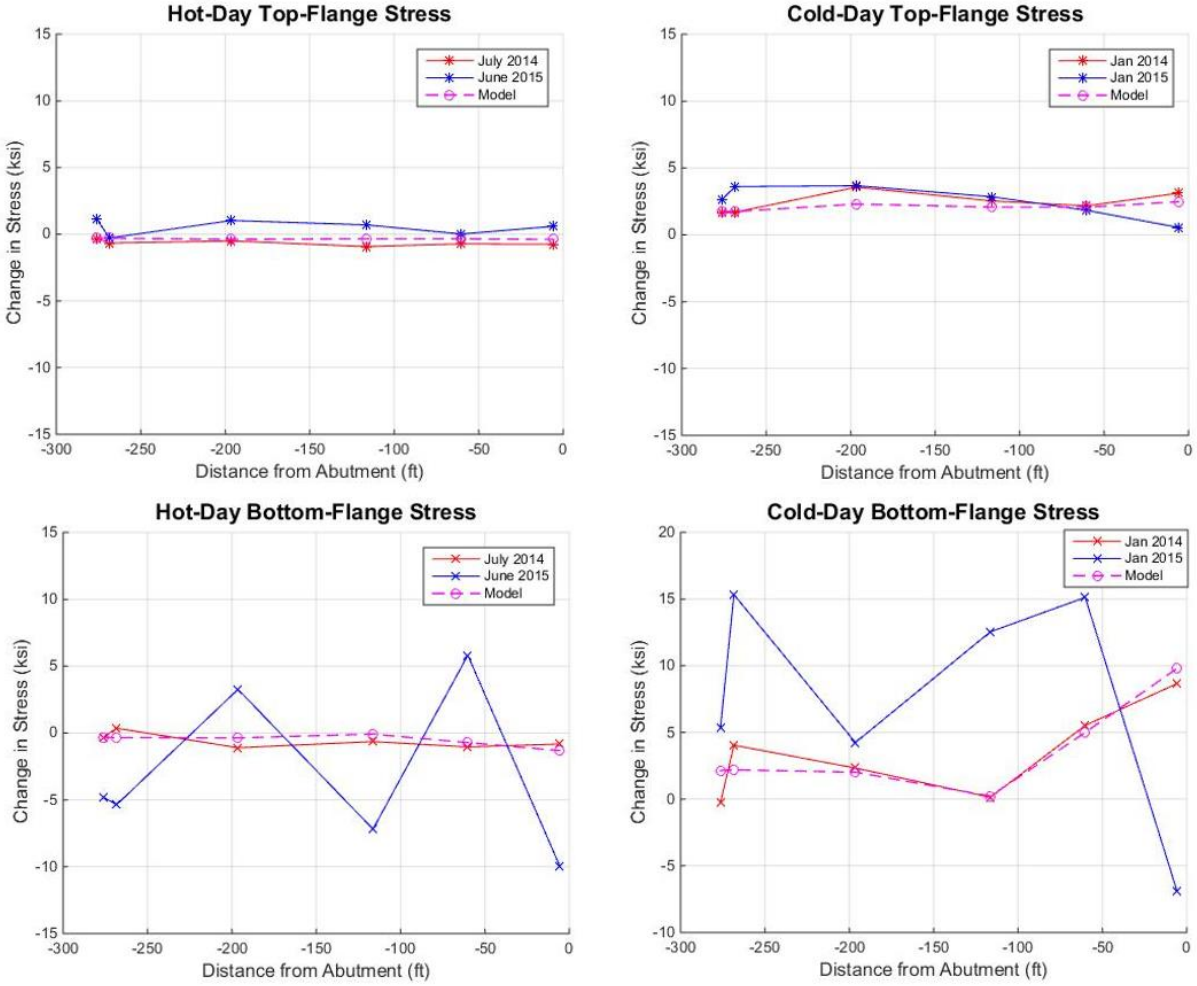

Figure 58. Hot and cold days field data and FE model comparison of Kishwaukee girder 2 stresses.

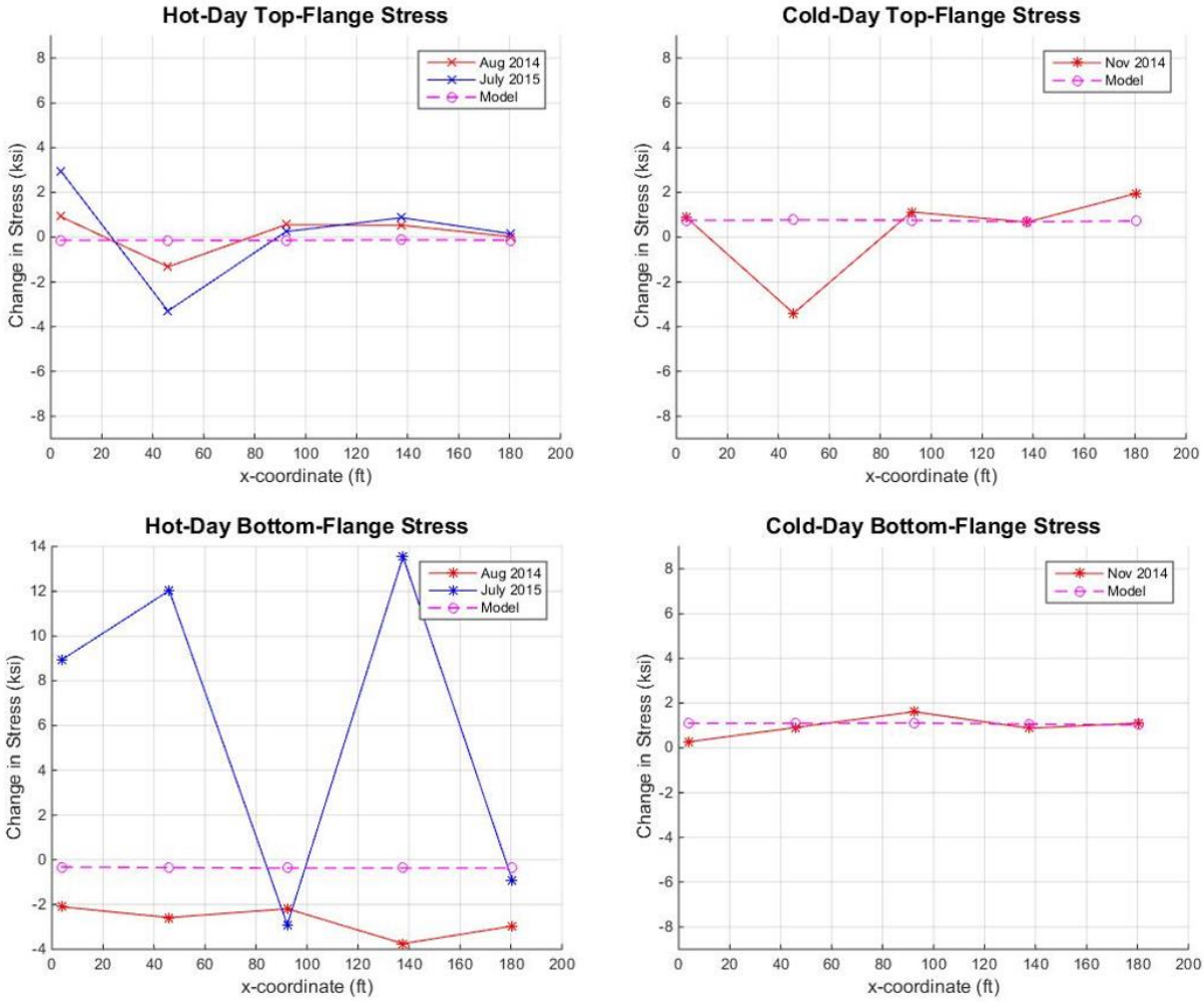

Figure 59. Hot and cold days field data and FE model comparison of UPRR girder 10 stresses.

CHAPTER 7: SUMMARY AND CONCLUSIONS

Field monitoring of two Illinois IABs, the Union Pacific Railroad (UPRR) Bridge and Kishwaukee River Bridge, was implemented to further investigate IAB behavior and supplement results from the preceding parametric study. The main objective of the field monitoring program was to investigate IAB superstructure behavior and validate modeling assumptions used in the project's different numerical models. Previous research regarding IABs has been largely focused on substructure behavior, leaving a gap in understanding of IAB superstructure behavior. Therefore, the instrumentation of the Kishwaukee and UPRR bridges was focused largely on the superstructure in hopes of providing further insight into superstructure behavior. Global movement, pile, girder, deck, and approach slab strains were monitored to assess IAB behavior and any build-up of thermal stresses. Rotations at different interfaces of the abutment were also monitored in order to assess modeling assumptions. Data was successfully collected for 16 months and 24 months at UPRR and Kishwaukee, respectively. In addition to the field monitoring, finite element numerical models were created of each of the instrumented bridges to provide a basis of comparison for further analysis of the field data and to validate and further investigate some of the modeling assumptions implemented.

Field monitoring results from both the Kishwaukee and UPRR bridges demonstrated clear trends in regard to IAB superstructure and substructure behavior. Data from all of the different gages installed exhibited clear tends with change in temperature. The calculated field abutment displacement of the Kishwaukee Bridge was slightly less than the theoretical free expansion/contraction and presented unsymmetrical movement of the bridge acute and obtuse corners, corroborating findings from the parametric study. This global movement was one of the main driving factors influencing pile and girder behavior. Field results typically showed higher magnitude pile strains near the acute corner, which is shown to have greater longitudinal displacements than the obtuse corner for such bridges with mild to high degrees of skew. Field pile strains correlated well with predictions from the models and both demonstrated the greatest strain contribution coming from weak-axis bending. Both the model and extrapolated field flange tip / extreme fiber pile strains were below yield strain and demonstrated there is typically some additional pile deformation capacity available, especially if limited pile yielding is allowed.

The most variable data resulted from the girders, particularly the bottom flange. Deck, girder top flange, and girder web stresses all showed clear trends with temperature and matched well with model predictions. As seen in the parametric study, both the model and field bottom flanges had the highest magnitude stress. The model and field bottom flange data correlated well during the initial 6 to 12 months of data collection, with support locations (abutment and/or piers) typically demonstrating the highest magnitude of stresses along the girders. However, bottom flange stresses increased in magnitude after the initial 6 to 12 months, no longer following the expected trends exhibited in the model. This behavior could be due to out-of-plane bending leading to localized yielding, live load, or other cyclic effects. However, one distinct cause for this behavior is not clear. Overall, the girders stresses showed clear trends with change in temperature, which mostly matched model predictions and are of significant magnitude that it is recommended they be considered in IAB design.

The field monitoring program also provided valuable data utilized to assess different modeling assumptions implemented in the parametric study models and instrumented bridge models. Essentially no differential rotation was observed between the top diaphragm and lower footing of the abutment at both bridges indicating that the abutment cold joint is virtually a rigid connection, therefore validating the use of a rigid connection in the models. At the abutment – girder connection some slight differential rotation was measured at both bridges. However, as compared to calculations for a pinned girder scenario, the rotations are small enough to indicate a fixed connection assumption is valid. Overall, results from the field monitoring program provided valuable insight into different aspects of IAB behavior and validated key modeling assumptions, demonstrating high potential for application of the parametric study and field monitoring results in future IAB design.

REFERENCES

Arsoy, S., R. M. Barker, and J. M. Duncan. 1999. "The Behavior of Integral Abutment Bridges." VTRC 00-CR3, Virginia Transportation Research Council, VA.

Burdette, E. G., E. E. Ingram, J. B. Tidwell, D. W. Goodpasture, J. H. Deatherage, and S. C. Howard. 2004. "Behavior of Integral Abutments Supported by Steel H-Piles." *Transportation Research Record: Journal of the Transportation Research Board* 1892:24–28.

Computers and Structures, Inc. (CSI). 2009. SAP2000 Advanced 14.1.0 Structural Analysis Program, Berkeley, CA. http://www.csiamerica.com/

Computers and Structures, Inc. (CSI). 2013. CSI Knowledge Base,. http://www.csiamerica.com/.

Dicleli, M. 2005. "Integral Abutment-Backfill Behavior on Sand Soil—Pushover Analysis Approach." *Journal of Bridge Engineering*, ASCE, 10(3):354–364.

Dicleli, M., and S. M. Albhaisi. 2004. "Effect of Cyclic Thermal Loading on the Performance of Steel H-Piles in Integral Bridges with Stub-Abutments." *Journal of Constructional Steel Research* 60:161–182.

Ensoft, Inc. 2005. LPILE Plus v.5.0 Geotechnical Analysis Program (Student Version), http://www.ensoftinc.com/.

Frosch, R. J., and M. D. Lovell. 2011. "Long-Term Behavior of Integral Abutment Bridges." Publication FHWA/IN/JTRP-2011/16. Joint Transportation Research Program, Indiana Department of Transportation and Purdue University, West Lafayette, Indiana. doi: 10.5703/1288284314640.

Han, Jarell. 2014. "Lateral Resistance of Piles near 15-Foot Vertical MSE Abutment Walls Reinforced with Ribbed Steel Strips." MS thesis. Paper 5320. Department of Civil and Environmental Engineering, Brigham Young University, Provo, UT.

Hassiotis, S., Y. Khodair, E. Roman, and Y. Dehne. 2006. "Evaluation of Integral Abutments." Final Report, FHWA-NJ-2005-025, New Jersey Department of Transportation and Stevens Institute of Technology, Hoboken, NJ.

Huang, J., C. French, and C. Shield. 2004. "Behavior of Concrete Integral Abutment Bridges." Minnesota Local Road Research Board. Report no. Mn/DOT 2004-43. Center for Transportation Studies, University of Minnesota, Minneapolin, MN.

"IDOT Memorandum: 2012 Integral Abutment Bridge Policies and Details." 2012. Illinois Department of Transportation Bureau of Bridges and Structures, 25 July 2012, http://www.idot.illinois.gov/Assets/uploads/files/Doing-Business/Memorandums-&-Letters/Highways/Bridges/ABD-Memos/abd123.pdf

Ingram, E. E., E. G. Burdette, D. W. Goodpasture, J. H. Deatherage, and R. M. Bennett. 2004. "Behavior of Steel H-Piles Supporting Integral Abutments," pp. 219–225. In *Proceedings of the ASCE Structures Congress*. Nashville, TN.

Khodair, Y. A., and S. Hassiotis. 2013. "Rigidity of Abutments in Integral Abutment Bridges." *Structure and Infrastructure Engineering* 9(2):151–160. DOI:10.1080/15732479.2010.541264.

Kim, W., and J. A. Laman. 2010. "Numerical Analysis Method for Long-Term Behavior of Integral Abutment Bridges," *Engineering Structures* 32(8):2247–2257.

Kim, W., and J. A. Laman. 2012. "Seven-year field monitoring of four integral abutment bridges." *Journal of Performance of Constructed Facilities*, ASCE, 26(1):54–64.

LaFave, J. M., L. A. Fahnestock, B. A. Wright, J. K. Riddle, M. W. Jarrett, J. S. Svatora, H. An, and G. Brambila. 2016. "Integral Abutment Bridges Under Thermal Loading: Numerical Simulations and Parametric Study." A report of the findings of ICT-R27-115. Illinois Center for Transportation Series No. 16-015. Research Report No. FHWA-ICT-16-014. Illinois Center for Transportation, Rantoul, IL.

Nelson, K. R. 2013. "Lateral Resistance of Piles near Vertical MSE Abutment Walls at Provo Center Street." MS thesis, Department of Civil and Environmental Engineering, Brigham Young University, Provo, UT.

Olson, S.M., J. H. Long, J. R. Hansen, D. Renekis, and J. M. LaFave. 2009. "Modification of IDOT Integral Abutment Design Limitations and Details," Illinois Center for Transportation Research Report, ICT-09-054. University of Illinois, Urbana, IL.

Olson, S. M., K. P. Holloway, J. M. Buenker, J. H. Long, and J. M. LaFave. 2012. "Thermal Behavior of IDOT Integral Abutment Bridges and Proposed Design Modifications." Illinois Center for Transportation Research Report, ICT-12-022, University of Illinois, Urbana, IL.

Paul, M.D., J. A. Laman, and D. G. Linzell. 2005. "Thermally Induced Superstructure Stresses in Prestressed Girder Integral Abutment Bridges." *Transportation Research Record: Journal of the Transportation Research Board*, CD 11-S:287–297. Transportation Research Board of the National Academies, Washington, D.C.

Price, J. S. 2012. "Lateral Resistance of Piles near Vertical MSE Abutment Walls." MS thesis, Department of Civil and Environmental Engineering, Brigham Young University, Provo, UT.

Quinn, B. H., and S. A. Civjan. 2017. "Parametric Study on Effects of Pile Orientation in Integral Abutment Bridges." *Journal of Bridge Engineering*, ASCE, 22(4): -1—1.

Shoukry, S. N., G. W. William, and M. Y. Riad. 2008. "Response of an Integral Abutment Bridge to Temperature Variations." In *Proceeding of Structures Congress*, Vancouver, British Columbia, Canada.

William, G. W., S. N. Shoukry, and M. Y. Riad, 2012. "Study of Thermal Stresses in Skewed Integral Abutment Steel Girder Bridges." *Structural Engineering International* 22(3):308–317.

Wright B., J. LaFave, L. Fahnestock, M. Jarrett, J. Riddle, and J. S. Svatora. 2015. "Field Monitoring of Skewed Integral Abutment Bridges*."* In *Proceeding of the joint 6th International Conference on Advances in Experimental Structural Engineering and 11th International Workshop on Advanced Smart Materials and Smart Structures Technology*, University of Illinois, Urbana–Champaign, United States, August 1–2, 2015.